Attribution of Arctic sea ice decline from 1953 to 2012 to influences from natural, greenhouse-gas and anthropogenic aerosol forcing

by

Bennit L. Mueller
B.Sc., RWTH Aachen University, 2010
M.Sc., RWTH Aachen University, 2013

A Thesis Submitted in Partial Fulfillment of the
Requirements for the Degree of

MASTER OF SCIENCE

in the School of Earth and Ocean Sciences

Attribution of Arctic sea ice decline from 1953 to 2012 to influences from natural, greenhouse-gas and anthropogenic aerosol forcing

by

Bennit L. Mueller
B.Sc., RWTH Aachen University, 2010
M.Sc., RWTH Aachen University, 2013

Supervisory Committee

Dr. N. P. Gillett, Co-Supervisor
(School of Earth and Ocean Science)

Dr. A. Monahan, Co-Supervisor
(School of Earth and Ocean Sciences)

Dr. F. W. Zwiers, Outside Member
(Department of Mathematics and Statistics)

ABSTRACT

By the end of 2016 surveillance and reconnaissance satellites will have been monitoring Arctic-wide sea ice conditions for decades. Situated at the boundary between atmosphere and ocean, Arctic sea ice retreat has been one of the most conspicuous indication of climate change, especially in the two most recent decades. The 2001 annual minimum extent of Arctic sea ice marks the last year above the 1981 – 2012 long-term average extent. Ever since then only lower than average Arctic sea ice has been observed at the end of each summer's melt season. For more than a century climate scientists have postulated that the darkening of the Arctic due to retreating sea ice and therefore more exposed open ocean would be the consequence of global warming. In the first decade of the 2000s the human influence on that warming in the Arctic was indeed detected in observations and attributed to increasing atmospheric greenhouse-gas concentrations. In this study we direct our attention to a potential offsetting effect from other anthropogenic (OANT) forcing agents, mainly aerosols, that has potentially out masked a fraction of greenhouse-gas induced warming by a combined cooling effect. We acknowledge that multiple sources of uncertainty exist in our method, in particular in the observed records of Arctic sea ice and corresponding simulations from climate models.

No formal detection and attribution (DA) analysis has yet been carried out to try to detect the combined cooling effect from aerosols in observations of Arctic sea ice extent. We use three publicly available observational data sets of Arctic sea ice and climate simulations from eight models of the Coupled Model Intercomparison Project Phase 5 (CMIP5). In our detection and attribution study observations are regressed on model-derived climate response pattern, or fingerprints, under all known historical (ALL), greenhouse-gas only (GHG) and known natural-only (NAT) forcing factors using an optimal fingerprinting method. We estimate regression coefficients (scaling factors) for each forcing group that scale the fingerprints to best match the observed record. From the scaled ALL, GHG and NAT fingerprints we calculate the relative contribution of the observed sea ice decline attributable to OANT forcing agent. Based on our DA results we show that the simulated climate response patterns to changes in GHG, OANT and NAT forcing are detected in the observed records of September Arctic sea ice extent for the 1953 to 2012 period.

Contents

Supervisory Committee **ii**

Abstract **iii**

Table of Contents **iv**

List of Tables **vi**

List of Figures **vii**

Acknowledgements **viii**

Dedication **ix**

1 Introduction **1**

2 Climate Change Detection and Attribution **3**

2.1 Detection and Attribution on Arctic Sea Ice 4

2.1.1 Multi- pattern Fingerprint Method for Detection and Attribution 5

2.1.2 Regularized Optimal Fingerprinting 7

2.1.3 Sea Ice Observations and Models 9

2.1.4 Sea Ice Modelling 11

2.2 Arctic sea ice variability 15

2.2.1 Perfect model experiment 17

3 Results **21**

3.1 Perfect model experiment results 21

3.2 Detection and Attribution results 25

4 Discussion **32**

Bibliography **35**

List of Tables

Table 2.1 List of CMIP5 model and corresponding ensemble size under GHG, ALL and NAT forcing 4
Table 2.2 Overview of eight selected GCMs and their atmosphere, land, ocean and sea ice sub-models 11
Table 2.3 CMIP5 models and processes included in the calculation of the other anthropogenic response 13

Table 3.1 Modelled and observed trends of Arctic sea ice decline 1953 - 2012 in September. 30
Table 3.2 Scaling factors β and 5-95% confidence intervals ($\beta_{low} - \beta_{up}$) and corresponding attributable trends (AT) 30

List of Figures

Figure 2.1 September Arctic sea ice extent under RCP 8.5 12
Figure 2.2 Mean September Arctic sea ice extent (lines) from 1953 to 2012 14
Figure 2.3 Mean September Arctic sea ice extent (lines) from 1953 to 2012, OANT signal 15
Figure 2.4 Model spread in CMIP5 piControl simulation 18
Figure 2.5 Ratios of variance 19
Figure 2.6 CanESM2 LE and CESM LE timeseries 20

Figure 3.1 Detection and Attribution results from CanESM2 LE PME . . 22
Figure 3.2 Detection and Attribution results from CESM1 LE PME 23
Figure 3.3 Detection and Attribution results 26
Figure 3.4 Detection results for individual models IV1 27
Figure 3.5 Detection results for individual models IV2 28
Figure 3.6 Attributable trends 31

We acknowledge the World Climate Research Programme's Working Group on Coupled Modelling, which is responsible for CMIP, and we thank the climate modelling groups for producing and making available their model output. For CMIP the U.S. Department of Energy's Program for Climate Model Diagnosis and Intercomparison provides coordinating support and led development of software infrastructure in partnership with the Global Organization for Earth System Science Portals. B.M. acknowledges funding from the Canadian Sea Ice and Snow Evolution Network (CanSISE). M. Piron, H. Titchner and J. Walsh are thanked for their comments on available observational data sets. J. Fyfe, N. Swart, G. Flato, R. Najafi, A. Dirkson and B. Johnson are thanked for their comments on earlier versions of the manuscript.

To my family and friends; longum iter est per praecepta, breve et efficax per exempla

Chapter 1

Introduction

One of the best quantified aspects of climate change in the Arctic is the monitoring of changes in the spatial extent of the sea ice with passive-microwave sensors on board of satellite systems since 1978. Satellite observations of the Arctic show a negative trend in sea ice concentration (SIC) in all seasons and all Arctic sub-regions except the Bering Sea for the 1979 to 2012 period [63, 7, 70]. The minimum sea ice extent (SIE) reached in September 2012 set a new low record following the earlier record set in 2007. All years past the year 2001 have SIE minima below the historical climatological mean conditions for the 1981 - 2012 period. According to the *National Snow and Ice Data Center (NSIDC)* higher than the long-term average Arctic temperatures have recently hampered new sea ice formation during the winter of 2015 resulting in the lowest ever observed annual maximum sea ice extent in March, 2016. The September SIE of 2016 was the fifth lowest in the satellite era and marks the 15th successive year with lower than average sea ice extent in the Arctic [9, 78]. Satellite observations of the modern era (1979- present) show a downward trend in spatial sea ice extent in all seasons - smaller in winter and larger in summer [63]. The September linear trend of Arctic ice decline stands at -12.4% per decade over the satellite record [69]. The decrease in spatial extent is accompanied by thinning of the sea ice [58, 38, 33, 35]. Thinner sea ice is affected more strongly by air- ice-ocean interaction allowing easier ice break-up, enhanced ice circulation, drift speed, and ice export rates out of the Arctic basin though the Fram strait [34]. The lateral shrinking and vertical thinning consequently lead to an overall loss in Arctic sea ice volume [7, 4].

Measurements of atmospheric aerosols imply a net negative radiative forcing due to increased burdens of atmospheric sulphate aerosols offsetting a fraction of recent global warming due to increased greenhouse-gas (GHG) concentration that would

have occurred otherwise [66]. Sulphur dioxide emissions, the aerosol's precursor gas, increased in the 1960s, 1970s and 1980s and then again in the 2000s [65, 66]. The combined effect from direct and indirect radiative effects associated with sulphate aerosols is a net cooling effect offsetting a fraction of the GHG induced warming over the past few decades [61, 56]. Indirect warming from decreasing aerosol burden after the 1980s and 2000s and continuously increasing greenhouse- gas induced warming have resulted in a net warming effect in the Actic [15, 17, 66, 11, 13, 46].

Based on climate model simulations conducted for the third phase of the Coupled Model Intercomparison Project (CMIP3), previous studies detected the relative anthropogenic (ANT) influence in the observed decline of Arctic SIE in the presence of natural (NAT) influences, mainly changing solar and volcanic activity, and internally induced climate variability (IV) [79, 20, 43, 27].

The concentration of tropospheric aerosols has increased since year 2000 [61, 66, 11]. Hence, it could be the case that part of the GHG-induced Arctic sea ice response is masked by this offsetting effect from tropospheric aerosols. It also implies that any future reduction in global aerosols emission could result in additional Arctic sea ice loss due to reduced aerosol cooling [13] and that the political declaration of intent to reduce global GHG emissions might not have the full anticipated effect. So far no formal detection and attribution (DA) study has addressed the question of a possible offsetting effect from other anthropogenic (OANT), mainly tropospheric aerosols, forcing and if it can be detected in the observed record of Arctic sea ice extent. In this DA study we follow up on this question using extended data records of the Arctic sea ice observations (1953 to 2012) that combine satellite observations and operational sea ice charts from multiple sources. We use climate simulations from eight models of the Coupled Model Intercomparison Project Phase 5 (CMIP5) under different climate forcing combinations.

In Chapter 2 the DA framework is explained in more detail by introducing the underlying statistical model and a brief description of available observations of Arctic sea ice and how they are constructed, followed by some remarks on sea ice modelling and aspects of using multi-model ensembles from intercomparison projects like CMIP5. Chapter 2 closes with a brief section on a perfect model experiment (PME) to study the sensitivity of the DA results to different estimations of internal climate variability. In Chapter 3 results from both the PME sensitivity test and the DA study on the offsetting effect from OANT forcing itself are presented. This is followed by a discussion of results and some concluding remarks in the final Chapter 4.

Chapter 2

Climate Change Detection and Attribution

To study the relative contribution of influences from natural (NAT), greenhouse-gas (GHG) and other anthropogenic (OANT; predominantly aerosol) forcing on the observed Arctic sea ice decline from 1953 to 2012 we use a detection and attribution (DA) technique referred to as regularized optimal fingerprinting (ROF) [22, 1, 53, 54]. This technique uses total least squares accounting for noise from internal (unforced) climate variability in both observed and simulated climate response. The ROF approach has been previously applied to changes in observed Arctic air temperatures and snow cover extent decline [46, 47]. In a 3-signal (GHG, ALL and NAT) ROF setup we regress the observed time series of Arctic SIE onto model-simulated response patterns (fingerprints). The regression coefficients scale the model-derived fingerprints (scaling factors) to best match the observations. If a scaling factor is positive and its 90% confidence interval (CI) is inconsistent with zero the associated fingerprint is said to be *detected* in observations. Scaling factors excluding zero and including unity indicate good agreement between observed and model-simulated climate response whereas negative scaling factors with large uncertainty bands would indicate a mismatch between simulated and observed climate response. Hence, if a scaling factor and its CI is consistent with unity and inconsistent with zero it maybe possible to attribute part of the observed change to the associated climate forcing. The relative contribution of OANT forcing agents has to be calculated from scaling factors corresponding to GHG, ALL and NAT fingerprints derived from available CMIP5 simulation under these forcing experiments (see Tab. 2.1). The sixth gen-

Table 2.1: List of CMIP5 model and corresponding ensemble size under GHG, ALL and NAT forcing

CMIP5 model	GHG	ALL	NAT
$BCC-CSM-1-1$	1	3	1
$CanESM2$	5	5	5
$CNRM-CM5$	6	10	6
$GISS-E2-H$	5	6	5
$GISS-E2-R$	5	6	5
$HadGEM2-ES$	4	3	4
$IPSL-CM5A-LR$	3	4	3
$NorESM1-M$	1	3	1

eration of CMIP, i.e. CMIP6, will include simulation under OANT forcing so that scaling factors can be estimated directly from corresponding simulation [52, 16].

[46] identified that a large portion of GHG induced Arctic warming has very likely been offset by the combined cooling effect of OANT forcing agents, mainly tropospheric aerosols. Any future decrease in atmospheric aerosol burden in the 21st century could therefore result in additional warming in the Arctic, which leads to an additional reduction in sea ice extent [13].

Following up on previous findings in this study we investigate if GHG-induced Arctic sea ice decline has been offset by the combined cooling effect of OANT forcing in a similar manner. We compare three available records of observed Arctic sea ice conditions with simulations from eight climate models using ROF [22, 1, 53, 54].

In the following sections detection and attribution, Arctic observations, the CMIP5 model simulation and assumptions regarding the temporal structure of internally generated climate variability are described in more detail.

2.1 Detection and Attribution on Arctic Sea Ice

Detection and attribution of Arctic sea ice change and its effects on the global climate contributes to our understanding of the physical scientific basis of climate change. In the context of *Climate Change detection and attribution* studies *detection* is the step of showing that a certain index of the climate system has changed over a given time in a statistical sense [25, 4, 83].

For example [43] detected human induced climate change in Arctic sea ice observations when analysing model data that included anthropogenic climate forcing.

The observations could not be explained by model simulation of the climate under natural-only forcing. Hence, the change signal was not detected in the latter case.

The *detection* step in the DA formalism involves the computation of regression parameters, or scaling factors, that adjust model simulated response patterns under a given forcing (i.e. fingerprints) to best match the observation. If a scaling factor of a fingerprint is significantly different from zero and positive, then that signal is detected in the observations. Negative scaling factors do not allow for a physical interpretation even if the associated confidence interval excludes zero. However, it might be an indication that important real world processes are not well captured in the model simulation or fingerprints from other forcings need to be considered in the DA study as well.

The second step in the DA framework is *attribution* that assesses the relative contributions of multiple plausible (i.e. in a known physical sense) change signals by assigning weights (scaling factors) to the different change signals and assigning statistical confidence [25]. If a fingerprint exceeds the observed signal (e.g., due to missing moderating forcing components) the analysis may produce a scaling factor less than unity to account for that mismatch and vice versa - if the simulated change is too small.

To increase confidence in the DA results it is common practice to use output from numerous climate models in an multi-model-ensemble (MME) setting instead of analysing single models individually. In the following we present the main DA results for the MME first, before discussing findings for individual climate models.

2.1.1 Multi- pattern Fingerprint Method for Detection and Attribution

In this DA study observed changes in Arctic September sea ice extent are attributed to the relative contribution of three climate forcings: GHG, NAT and OANT. The DA framework uses an adaptation of the total least-squares based optimal fingerprinting method [22, 23, 1].

Standard optimal fingerprinting consists of the generalised linear regression model

$$y_i = \sum_{i=1}^{l} \beta_i x_i + \epsilon \tag{2.1}$$

where y_i is the vector of the observations, x_i is the ith response pattern under

external climate forcing and β_i are corresponding unknown scaling factors. The ϵ term denotes internal climate variability. The model is then used to estimate β_i (scaling factors) to scale the amplitude of the response patterns to best match the observations. It is assumed that ϵ is a Gaussian random variable with covariance $C = Cov(\epsilon)$. The second assumption is that the climate response to multiple forcings is additive [18, 53].

Climate Change DA using Ordinary Least Square (OLS) approaches assume that the vector of the forced climate response x_i is perfectly known. In contrast, the Total Least Squares (TLS) approach accounts for uncertainties in both observations and climate model simulations. Hence both vectors y_i and x_i are not perfectly known and are represented as

$$y_i = x_i\beta + \epsilon_{y_i} \tag{2.2}$$

$$x_i = x_i + \epsilon_{x_i} \tag{2.3}$$

where ϵ_{y_i} is error in the observed record (i.e., internal climate variability) and ϵ_{x_i} is the unknown component in the climate model simulation. Furthermore, it is assumed that

$$\epsilon_{y_i} \sim \mathcal{N}(0, \Sigma_{y_i}) \tag{2.4}$$

$$\epsilon_{x_i} \sim \mathcal{N}(0, \Sigma_{x_i}) \tag{2.5}$$

assuming that $\epsilon_{y_i} - \epsilon_{x_i}$ is i.i.d. $\mathcal{N}(0, \Sigma)$. Both estimates of the covariance matrix of internal variability Σ_{y_i} and Σ_{x_i} are estimated either from unforced control simulations or from transient ALL forcing runs after the ensemble mean response has been removed.

Here we use a TLS- based fingerprinting method to estimate scaling factors for simulated GHG-, OANT- and NAT- induced response patterns to best match the observed records of Arctic September SIE. This method involves the estimation of the covariance matrix of internal climate variability C, the estimation of the scaling factors β_i, the associated uncertainty estimation and a consistency test on the regression residuals. Both steps require the matrix C to be known. In reality this matrix is not known exactly and has to be estimated. This estimate $\widehat{C}$ is constructed from

unforced control simulations [26, 24, 67, 43, 47]. The estimation of a well-conditioned covariance matrix $\widehat{C}$ is key in the DA formalism.

Similar to the approach used by [46] based on [23, 75, 1] we derive scaling factors for GHG, OANT and NAT from simulations under GHG, ALL and NAT. First the regression is carried out for the available response patterns to estimate scaling factors for GHG, ALL and NAT. In an second step response to ALL forcing in the initial regression model (Eq. 2.6) is decomposed assuming linear additivity

$$SIE_{obs.} = \beta_1 SIE_{ALL} + \beta_2 SIE_{NAT} + \beta_3 SIE_{GHG} + \epsilon \tag{2.6}$$

and SIE_{ALL} is substituted with

$$SIE_{ALL} = SIE_{GHG} + SIE_{NAT} + SIE_{OANT} \tag{2.7}$$

Then the scaling factors for GHG, OANT and NAT can be written as

$$\beta_{GHG} = (\beta_1 + \beta_3), \beta_{NAT} = (\beta_1 + \beta_2), \beta_{OANT} = \beta_1 \tag{2.8}$$

If the associated scaling factor of a response pattern is statistically significantly different from zero, then that signal is detected in the observations. If the scaling factor is close to unity it means that the observed change is consistent with the estimated model response to ALL, NAT and GHG forcing respectively. Discrepancies between the simulated and observed signal amplitudes may also indicate the existence of physical processes that are not well resolved in the models leading to structural biases between observations and simulations [45, 1].

2.1.2 Regularized Optimal Fingerprinting

As for other climate change DA applications, in this study one of the key difficulties in applying the fingerprint method is the computation of the the inverse of the covariance matrix of internal variability C. Its estimate from control data might not be invertible (i.e. singular) in the case where the available number of control run years for the estimation of $\widehat{C}$, n, is smaller than the number of data series from control runs p. In

this case a common practice is to reduce the dimension of the detection space. This can be achieved by making use of an empirical orthogonal function - (EOF) truncation of C. This allows for the computation of a pseudo- inverted version of the variance-covariance matrix of internal variability, namely the Moore-Penrose pseudo invert, $\widehat{C}_q^{\dagger}$ where q is the truncation parameter and dimension of the reduced detection space [21, 43, 51, 28].

One unfavourable property of a Moore-Penrose pseudo-inverse of the covariance matrix is that smallest, or high order, eigenvalues of $\widehat{C}_q^{\dagger}$ are underestimated whereas the biggest, or low order, eigenvalues are over-estimated. These errors are amplified when computing the inverse of $\widehat{C}_q^{\dagger}$ which can result in an ill-conditioned covariance matrix [51, 53].

In this study we use a regularization technique to ensure that the covariance matrix of internal variability is invertible. We use two different dataset to estimate internal variability. In both cases the regularized estimates has better properties (i.e. more accurate and lower sampling variability) [36, 51].

The main thrust behind this regularization technique is to find a covariance matrix estimate $\widehat{C_I}$, also known as the Ledoit estimate [36] of the form

$$\widehat{C_I} = \gamma \widehat{C} + \rho I_p \tag{2.9}$$

where I_p is the p x p identity matrix and γ and ρ are real numbers. Multiple methods to find the relevant estimators γ and ρ exist. We follow the method described in [51] (Appendix A1-A8 of that study) based on the initial method by [36].

Adding a scaled version of I has the benefit that the smallest eigenvalues in $\widehat{C_I}$ are now overestimated by decreasing the relative weight of high order eigenvalue providing a more stable DA algorithm when computing the inverse of $\widehat{C_I}$. Due to the use of this regularisation scheme this DA algorithm is referred to as *Regularized Optimal Fingerprinting* [53, 54].

After estimating the signal amplitudes the last step in ROF is to conduct a residual consistency test (RCT) to check if the estimated regression residuals are consistent with the climate model noise represented by a second estimate of the covariance matrix of internal variability. The second set is constructed by dividing the initial

full set of available control run segments into half. After removing all externally-forced signals in the regression procedure the regression residuals should be consistent with internal variability. The computation of the RCT test statistics involves a F-test between ratios of variances of the regression residuals and estimated internal variability. If the test statistic produces p-values between 0.05 and 0.95 (90% CI) the test is passed [1, 59]. Alternative version of the RCT procedure adopted for ROF that does not rely on parametric distributions is presented in [53].

Passing the RCT indicates that the overall assumptions of the statistical model hold. The test fails if at least one underlying assumption is violated, e.g. if the estimated internal variability is too low or there is no linear relationship in the response pattern. A detailed description of the RCT is given in [1] and [53].

2.1.3 Sea Ice Observations and Models

Due to the extensive size and inhospitable nature of the Arctic, spatially complete observations of sea ice concentration only began with the satellite era. However, multiple records of local SIC condition and ice edge position exist for the pre-satellite era from 1953 onward. They come from various sources with different resolutions and various spatial and temporal coverage. Global coupled climate model (GCM) simulation of sea ice under ALL, GHG and NAT forcing conducted for CMIP5 end in the year 2012 [69]. In this study we use time series of Septmeber Arctic SIE representing the annual minimum for the 1953 to 2012 period. For this period both observations and model simulations exist. For simulations and observed records of SIC, SIE is calculated as the area sum of grid cells with at least 15% SIC. The observational record produced by [48] consists of values of monthly mean SIE values.

We are using time series of the annual Arctic sea ice minimum represented by the mean September SIE as climate diagnostic.

We use three different publicly available observational data sets that all differ in processing of the raw remote sensing data or the assimilation techniques of data from various sources.

Two common procedures to derive sea ice products from the raw remote sensing data are the The National Aeronautics and Space Administration (NASA) Team sea ice algorithm [73] and the NASA Bootstrap algorithm [6]. In both cases surface brightness temperature measurements by the Special Sensor Microwave/ Imager (SSM/I) instrument are mapped onto discrete grids from which first- and multiyear

ice concentrations are calculated. The sum of both results in the overall SIC that is used to calculated SIE.

For the pre-satellite era various sources of information on the Arctic sea ice condition exist in the form of operational charts that mapped the ice edge position for navigation purposes. Although often locally and temporally constrained, operational sea ice charts provide one of the few archives of pre-satellite sea ice records. Their quality is not only limited by the areal coverage provided but also subject to the expertise of the navigation analyst who mapped the local sea ice condition during a cruise [62]. Errors in ice edge location in the The Arctic and Antarctic Research Institute (AARI) charts issued before 1998 vary from $2-10km$ [50] to $50km$ [39]. This is tolerable for our approach given that the calculation of the Arctic-wide September mean SIE is a large simplification and the effect of mapping inaccuracy is considered marginal compared to that.

In this study we make use of three available records of Arctic sea ice that were extended backwards into the the pre-satellite era by combining multiple data sources of different resolution, spatial and temporal coverage. For times and regions where observations from multiple sources exist, researchers applied a ranking scheme to determine the most accurate one [81]. We do not extend our study into years prior to 1953 as Arctic-wide coverage can only be achieved by making use of climatological infill where data gaps occurred.

In 2016 Walsh and Chapman released an updated version of *Gridded Monthly Sea Ice Extent and Concentration fields from 1850 onward (Version 1.1)*, WC hereafter [10]. The WC compilation is the only Arctic-wide record under investigation that incorporated sea ice information in the Russian sector from naval operational ice charts provided by the The Arctic and Antarctic Research Institute (AARI) covering 1933–2006 [80, 5, 39, 81].

The second set of sea ice observations is the newest update of the *Hadley Centre sea ice and sea surface temperature data set (HadISST.2.2.0.0)*, HadISST2 hereafter. The data for the 1953 to 1978 pre-satellite era rely mainly on an earlier version of WC that did not yet include the AARI data. Between 1995 to 2007 National Ice Centre (NIC) sea ice charts were used as reference to adjust SIC biases between the different data sources [76].

A third data set that came to my attention provides a *new time series of September Arctic sea ice extent from 1935 to 2014* [48]. The authors, Piron and Pasalodos (PP), include additional data for the Siberian sector of the Arctic that have not been used

previously in the existing Arctic wide time series. This dataset also includes an adjustment of a discontinuity in the sea ice record at the 1978 – 1979 boundary marking the switch from single- to multichannel microwave sensors on board the Nimbus satellite systems [41, 48].

It is striking that the trend of Arctic SIE in September is -12.9% per decade for most parts of the satellite period considered here (i.e. 1979 to 2011), which is nearly double the trend from 1953 to 2011 of -6.8% per decade relative to the 1981 to 2010 mean [41]. The combination of various data sources cannot guarantee perfect consistency across the entire analysis period. The consistency within the observed records is limited by the the lack of spatially complete data, data of different quality and resolution, and human judgement within individual products such as sea ice charts. The interpretation of the fact that the doubling of the declining rate coincides with the transition between the pre- and post-satellite era would deserves additional investigation.

2.1.4 Sea Ice Modelling

Besides Arctic sea ice observations we analyze simulations from eight CMIP5 climate models covering the 1953 – 2012 period under historical GHG forcing, natural changes in NAT and under the combined effect of ALL forcing included in the models. In some cases the historical ALL simulation ended in 2005 and we extended these to the year 2012 with ALL forcing extended simulations provided by the associated modelling centres or with *Representative Concentration Pathway 4.5 simulations* (RCP4.5) representing a moderate assumption of additional radiative forcing of $4.5 Wm^{-2}$ by the end of the 21st century relative to the 1750 reference. An overview of models used in this study is shown in Table 2.2.

Model	Atmosphere	Land	Ocean	Ice	*ALL*	*NAT*	*GHG*
BCC-CSM1.1	BCC-AGCM2.1	CLM3	MOM4	GFDL SIS	3	1	1
CanESM2	AGCM4	CLASS	NCAR	CanSIM1	5	5	5
CNRM-CM5	ARPEGE	ISBA	NEMO-OPA	GELATO	10	6	6
GISS-E2-R	GISS	GISS	Russel OM	Russel OM	6	5	5
GISS-E2-H	GISS	GISS	HYCOM	HYCOM	6	5	5
HadGEM2-ES	HadGAM2	TRIFFID	HadGOM2	n/a	3	4	4
IPSL-CM5A-LR*	LMDZ	ORCHIDEE	NEMO-OPA	NEMO-LIM	4	3	3
NorESM1-M	CAM4	CLM4	MICOM-HAMOCC	CICE	3	1	1

Table 2.2: Overview of eight selected GCMs and their atmosphere, land, ocean and sea ice sub-models. Also the number of available simulations under historical (ALL), natural-only (NAT) and greenhouse-gas (GHG) forcing. Asterisk denotes RCP4.5 extension. List of acronyms is provided by [60, and references therein]

Despite providing sufficient simulations from 1953 – 2012 under GHG, NAT and ALL forcing the *CSIRO-MK-360* model was excluded from all analysis because of its unrealistic Arctic sea ice simulation [40, 77]. The *CSIRO-MK-360* model simulates excessive sea ice in the winter month due to a filter parameter that regulates spurious ice-ocean fluxes between the ocean and sea ice models. It decreases the ice-ocean stress which increases the ice formation and slows down the decline of the ice cover throughout the 21st century [19]. Its outlying characteristic compared to the majority of the CMIP5 model population is shown in Figure 2.1.

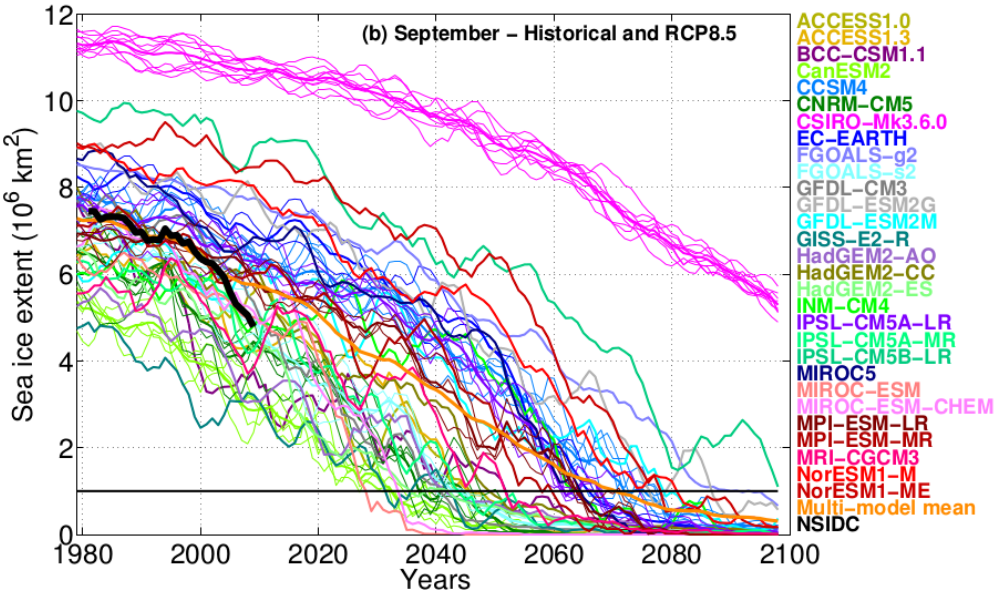

Figure 2.1: September Arctic sea ice extent (5-yr running mean) as simulated by 29 CMIP5 models. The historical runs are merged with the RCPs (representative concentration pathways RCP 8.5) Members of the same model, if more than one, are represented by thin lines. Individual models (or the mean of all their members,) are represented by thick lines. The multi-model mean (equal weight for each model) is depicted by the thick orange line. Observations are shown as the thick black line. The horizontal black line marks the 1 million km^2 September sea ice extent threshold defining ice-free conditions in this paper. Modified after [40].

A noticeable structural difference among the eight CMIP5 models exist in the way their aerosol schemes are designed (Table 2.3). *NorESM1-M* is the only model that includes time varying ozone in the GHG simulations in contrast to all other climate models that only include well-mixed greenhouse-gases. The climate response to changes in ozone concentration is therefore included in the GHG simulations. This has the negative effect that the ozone signal will get subtracted in the approach to

derive the OANT response (see Eq. 2.7).

CMIP5 Model List										
Model	Oz	SD	SI	BC	OC	LU	SS	Ds	MD	AA
BCC-CSM	yes	yes	no	yes	no	no	yes	yes	no	no
CanESM2	yes	yes	yes	yes	yes	yes	no	no	no	no
CNRM-CM5	yes	yes	yes	yes	yes	no	no	no	no	no
GISS-E2-H	yes	yes	yes	yes	yes	yes	no	no	no	no
GISS-E2-R	yes	yes	yes	yes	yes	yes	no	no	no	no
HadGEM2	yes	yes	yes	yes	yes	yes	no	no	no	no
IPSL-CM5A	yes	yes	yes	yes	yes	yes	yes	no	yes	yes
NorESM	no	yes	yes	yes	yes	no	no	no	no	no

Table 2.3: Eight selected CMIP5 models and processes included in the calculation of the other anthropogenic (OANT) response resolving relative radiative effects from Ozone (Oz), effects from sulphate aerosols, direct (SD) and indirect (SI), black carbon (BC), organic (OC), changes in land use (LU), sea salt (SS), dust (Ds), mineral dust (MD) and anthropogenic aerosols (AA). Modified after [74] and [8].

We calculate the CMIP5 multi-model ensemble (MME) mean response by giving equal weight to each model thereby not accounting for notable differences in individual ensemble sizes, i.e. largest: 10, smallest: 1 (see Fig. 2.2). Figure 2.2 shows an overview of the model simulated Arctic sea ice response. Visible spikes of increased SIE in ALL and NAT simulations correspond well with increasing sulphate (SO_4) burden in the stratosphere after the three most recent major volcanic eruptions from Mt. Agung (1963), El Chichón (1982) and Mt. Pinatubo (1991) indicating that the CMIP5 sea ice models are able to simulate temporary weakening of the spatial sea ice decline due to aerosol cooling. The SIE response to OANT forcing is derived by subtracting the signals from GHG and NAT from simulations under ALL forcing (Figure 2.3). Since most CMIP5 model provide a larger number of historical ALL forcing simulations than under GHG and NAT forcing, the overall ensemble size of every climate model is reduced to the smallest shared ensemble number under all three forcing experiments. Figure 2.3 illustrates that in first half of the observational Arctic sea ice record the GHG and OANT response are working in opposite direction. The linear trend of Arctic sea ice extent in response to OANT forcing is positive for the 1953 to 2012 period. When considering only the satellite era (1979 to 2012) the linear trend of Arctic sea ice extent is negative ($-0.004[10^6 km^2 a^{-1}]$). Therefore we

include pre-satellite observation to our DA analysis from times where the GHG and OANT response were less collinear than for the majority of the satellite record.

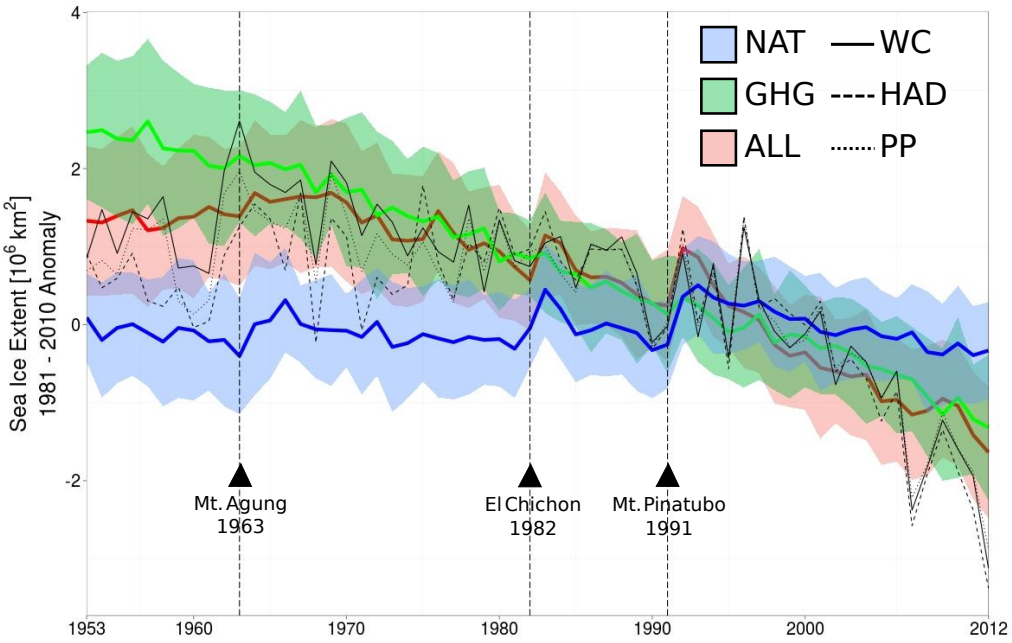

Figure 2.2: Mean September Arctic sea ice extent (lines) from 1953 to 2012 across all members from eight CMIP5 model ensembles under ALL,GHG and NAT forcing and ± one standard deviation (envelope) and the 1981 - 2010 sea ice anomaly from three available observed datasets (WC, HadISST2, PP).

Spatial changes of the sea ice can be monitored quite readily by the means of satellites. The sea ice pack can undergo sizeable volume losses that would not be apparent when only regarding SIE as index. Spatial SIE and SIT can be utilized to estimate the total volume of the ice pack. Changes in sea ice volume are mainly driven by two sets of processes. The first consists of thermodynamic processes that modulate the rate of heat exchange at the atmosphere- ice and the ice- ocean interfaces as well as the ice internal heat fluxes. Thermodynamic processes mainly control the amount of vertical and lateral ice growth and melt. Dynamic processes, in contrast, predominantly redistribute ice mass by either horizontal and vertical transport due to wind or ocean currents. They also have the potential to cause deformation of the ice by changes in internal stress. The GCMs participating in CMIP5 resolve relevant components of the climate system in their model components (e.g. atmosphere, land, ocean, ice) but structural differences in these components exist between the models

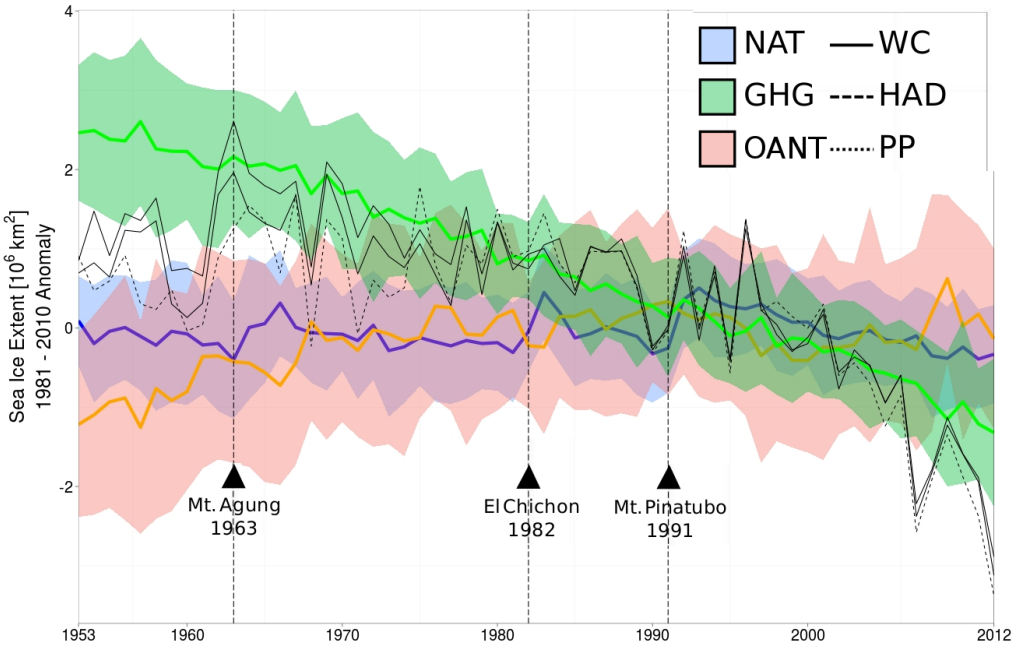

Figure 2.3: Mean September Arctic sea ice extent (lines) from 1953 to 2012 across all members from eight CMIP5 model ensembles under GHG, NAT and OANT forcing and ± one standard deviation (envelope) and the 1981 - 2010 sea ice anomaly from three available observed datasets (WC, HadISST2, PP).

(Tab. 2.2).

2.2 Arctic sea ice variability

Observed variables of the Earth system are subject to natural internally generated variability. This IV arises from the coupled, complex and highly non-linear nature of the Earth system e.g. from atmospheric and oceanic turbulence and various feedback mechanisms. Large ensembles (LE) of sea ice simulations with different initial conditions provide an unprecedented large sample of IV of the underlying climate [72]. The first LE experiment considered here is the CESM Large Ensemble Project. This 35-member LE is produced with CESM1(CAM5) under historical ALL forcing for the 1920 to 2005 period. Thereafter the *Representative Concentration Pathways* assuming an additional radiative forcing of $+8.5 W/m^2$ by the year 2100 (RCP8.5) is used. It lies in the nature of GCMs such as CESM and CanESM2 that small perturbations in the initial conditions grow rapidly over time [57]. The spread in the LE is gener-

ated using round-off differences in the initial conditions of the atmospheric state[30]. The second LE experiment was conducted by the *The Canadian Centre for Climate Modelling and Analysis* (CCCma) using the CanESM2 model under historical ALL forcing. Five initial ensemble members were each branched in the year 1950 into ten descendent runs, producing a 50-member LE. The ensemble spread in all members can then be taken as a measure of IV. To study the sensitivity of the DA results to the choice of how internal climate variability (IV) is prescribed in the ROF approach we estimate two separate sets of climate variability, IV1 and IV2.

The first estimate of internal variability, IV1 is constructed from 408 non-overlapping segments of $\sim 24,500$ years of control simulations carried out by 54 CMIP5 models under constant pre-industrial, i.e. pre-1850, (piControl) climate forcing. Figure 2.4 shows the conditional relationship between mean sea ice extent and the sea ice variability (i.e. standard deviation in this case) for the CMIP5 models. Despite possible model interdependency within the CMIP5 population [60] no obvious clustering of model subgroups seems apparent. Models that have the highest relative weight (in Fig. 2.4, longer simulations indicated by darker colors) when estimating IV from their control simulations are spread out quite evenly in the full CMIP5 population.

The second set, IV2 comes from simulation under transient ALL forcing from two large ensemble experiments. Comparing two structurally different datasets of IV allows us to test the influence on the DA results when using a sample estimate of IV that does not account for transient non-stationary changes in response to anthropogenic forcing (IV1) in contrast to a sample estimate of IV from transient ALL forcing runs (IV2). The second set of non-stationary internal variability (IV2) is produced by centering all 85 LE members by subtracting the LE mean response to ALL forcing (see Fig. 2.6). Figure 2.5 illustrates the emergence of increasing internal variability in transient LE runs in comparison to control simulations with constant forcing from the same two climate models. The nonstationarity emerges in the first three decades of the 21st century indicated by variance ratios diverging from a horizontal uniform band. For CanESM2 it is striking that the variance ratios in the second half of the 20st century are consistently lower than unity. The overall ratio between the mean variance across all CanESM2 LE members and variance from a corresponding CanESM2 control run (1,096 years) is only 0.77 for the 1950 to 2000 period indicating higher variability in LE historical ALL forcing simulations than in the control simulation under pre-industrial forcing. Since the mean Arctic SIE in September for the 1950 to 2000 period is similar (i.e. 5.17 million km^2 for CanESM2 LE and 5.06 million

km^2 CanESM2 control run) the difference in variability may not be explained by the conditional mean SIE alone and must arise in the simulations itself. It may well be that IV is different under weaker climate forcing in pre-industrial control simulation. A thorough discussion of the possible reasons for this behaviour would be beyond the scope of this thesis. However, some considerations of model and observation biases and comparing metrics on simulations from CanESM2 and CanESM2 LE are given in [40, 42, 64, 3].

2.2.1 Perfect model experiment

In order to study sensitivity of DA results to non-stationary IV a perfect model experiment (PME) is carried out. Using only one model in a PME has the benefit of reducing the influence of uncertainty associated with differences in model forcing, observational uncertainty and structural model differences inherent to multi-model-ensembles like CMIP5.

In the PME a one- signal test case is created where the DA algorithm is used to detect a fingerprint derived from all-but-one LE members in "observations" which are represented by the remaining one member. First, similar to fingerprinting methods from other DA studies [44, 59, 49, 46, 47], a time- adjusted version of IV1 is used (i.e. matching the length of the DA analysis period). Then the experiment is repeated using time- adjusted versions of IV2. The standard deviation of control simulation is $0.357[10^6 km^2]$ for CanESM2 and $0.270[10^6 km^2]$ for CESM1 which falls close to the mean standard deviation from all 54 CMIP5 models ($0.346[10^6 km^2]$) that contribute simulations to estimate IV1. Arguably, it would be a fairer comparison if IV1 would be estimated from control simulations from CanESM2 and CESM1 only. However, this would provide only a fraction of available control run segments compared to the full CMIP5 archive to estimate IV. Also, using control simulations from multiple CMIP5 models to estimate IV is common practice in the recent DA literature [29, 32, 14, 59, 82, 46]. Here, we assess this practice and its suitability for DA on Arctic sea ice extent. The PME is repeated for four different analysis periods to document if and when the DA results are effected by the choice of the estimate of IV. Difference in the DA results are manifested in the scaling factors and their 90% CI as well as the success rate of the RCT. The expectation is that in a PME the failure rate for the RCT (using a 90 % CI) is about 10% of the total.

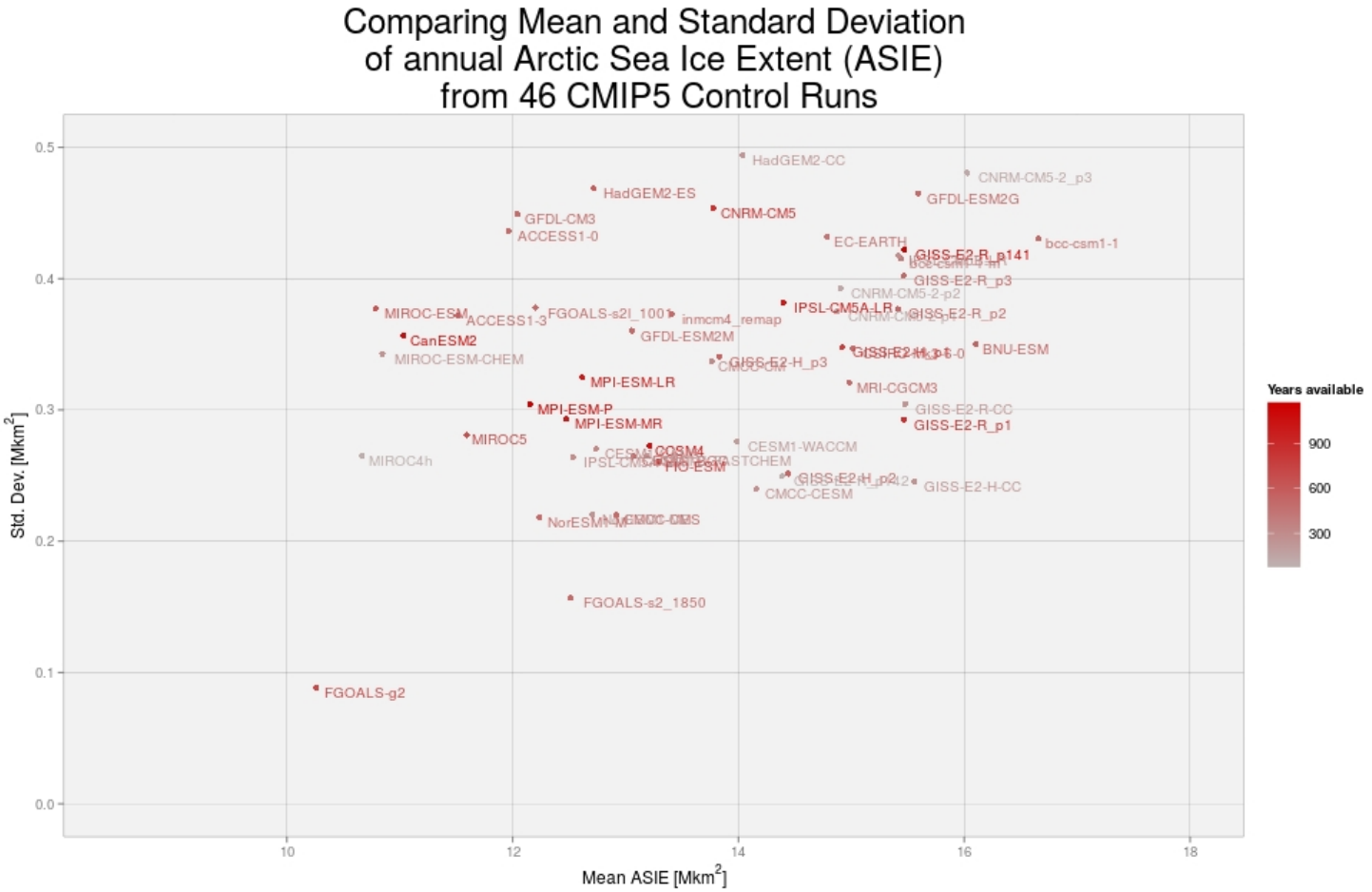

Figure 2.4: Standard deviation represented as a function of the mean Arctic SIE from 46 realisations from CMIP5 unforced pre- industrial control (piCintrol) experiment.

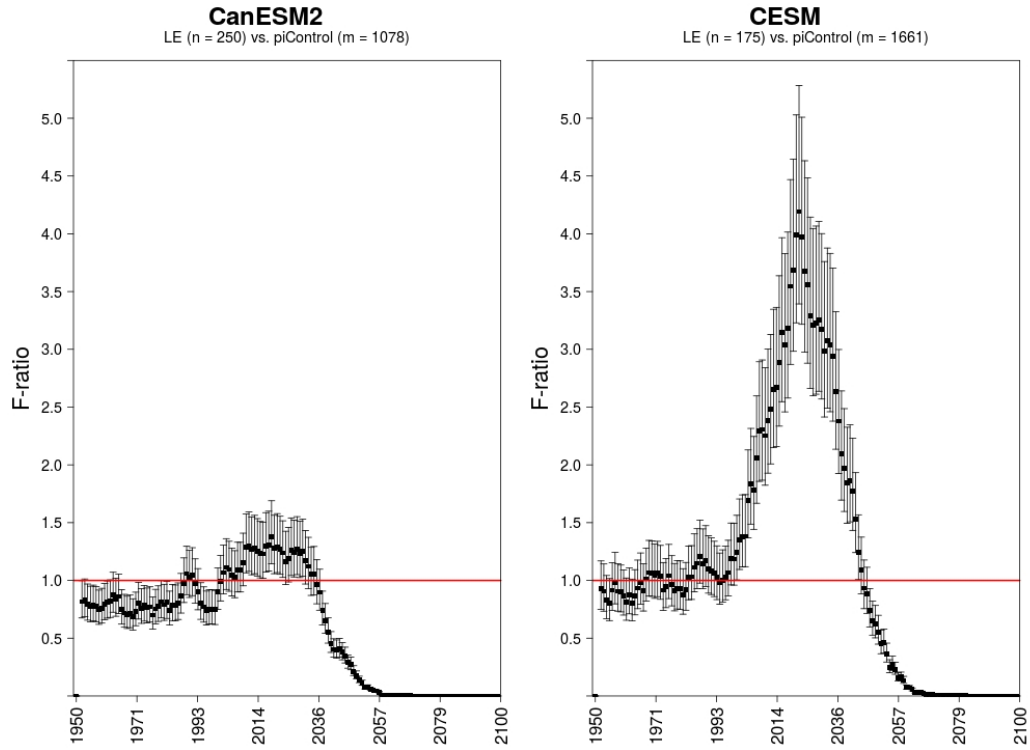

Figure 2.5: Ratios of variance between simulations under historical ALL (1950 – 2005) and RCP8.5 (2006 – 2100) forcing and corresponding unforced control simulation with constant pre-industrial forcing for CanESM2 LE (left) and CESM LE (right). After removing the LE mean response to ALL forcing from every individual ensemble member a 5-year rolling window at every simulation year is summed up across all available LE member to create a sample of 250 (175) for CanESM2 (CESM) simulation years that is representative for a given timestep. From that sample of representative years the variance is calculated. The variance for each set of simulation years is then divided by the total variance calculated from a corresponding control run from the same climate model. That way we the obtain variance ratios and associated confidence intervals at the 95 % confidence level. The horizontal line at unity denotes equality of variances. In CanESM2 LE simulations the variance for the 2000 – 2030 period is roughly 1.5 times higher compared to the 1950 – 1990 period. Variance in CESM LE simulations reaches is three to four times higher when comparing the two periods. In both cases variance ratios converges towards zero after 2040 as the Arctic becomes seasonal ice free in both models and variance vanishes.

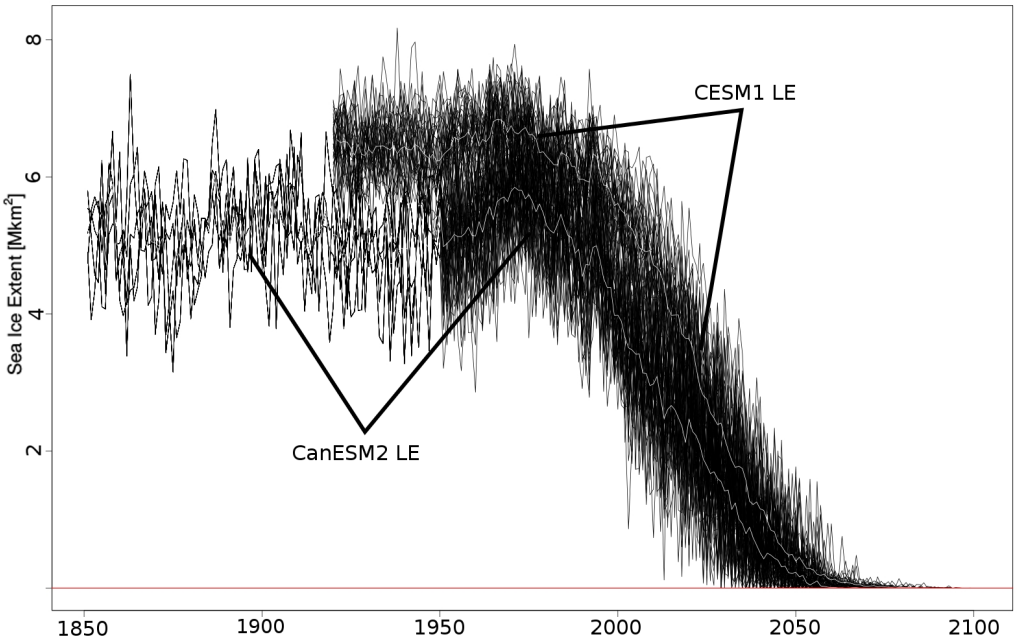

Figure 2.6: Individual simulations (black) and ensemble mean (white) of Arctic sea ice extent in September from CanESM2 LE and CESM LE under historical ALL forcing from 1850 to 2100.

Chapter 3

Results

3.1 Perfect model experiment results

Results from the proposed PME using the two available LE datasets (CanESM2 LE, CESM LE) are presented in Figure 3.1 and Figure 3.2. Both figures are structured into four panels each representing different analysis periods. Dots represent the estimated scaling factor β while whiskers illustrate the associated 90% confidence intervals ($CI90$). Black colors are used for results using CMIP5 control runs to estimate internal variability. Red colors are used when IV was estimated using LE residual variability. The residual consistency test score (RCTS) indicates the success rate of passing the test for both choices of IV.

In the first period from 1950 to 2005 in CanESM LE the ALL response from any individual LE members is detected in the ensemble mean of remaining members. When using CESM LE three cases exist where an LE member is not detected in the ensemble mean response. Uncertainty in the estimated scaling factors is also largest for this period for both models. Overall the differences in the DA results appear to be unsystematic. The RCTS seems not to depend on the choice of IV in CanESM2 LE whereas it is six times higher in CESM LE when transient IV2 is used instead of stationary IV1.

In the second analysis period from 1950 to 2020 the ALL signal is detected in all cases for both models. Also a noticeable decrease in uncertainty in the estimated scaling factors is visible across both LEs. Again, differences between the two models exist (e.g., for CanESM2 LE scaling factors overall seems to be in closer agreement with unity than for CESM LE) but they do not seem to follow systematic structure.

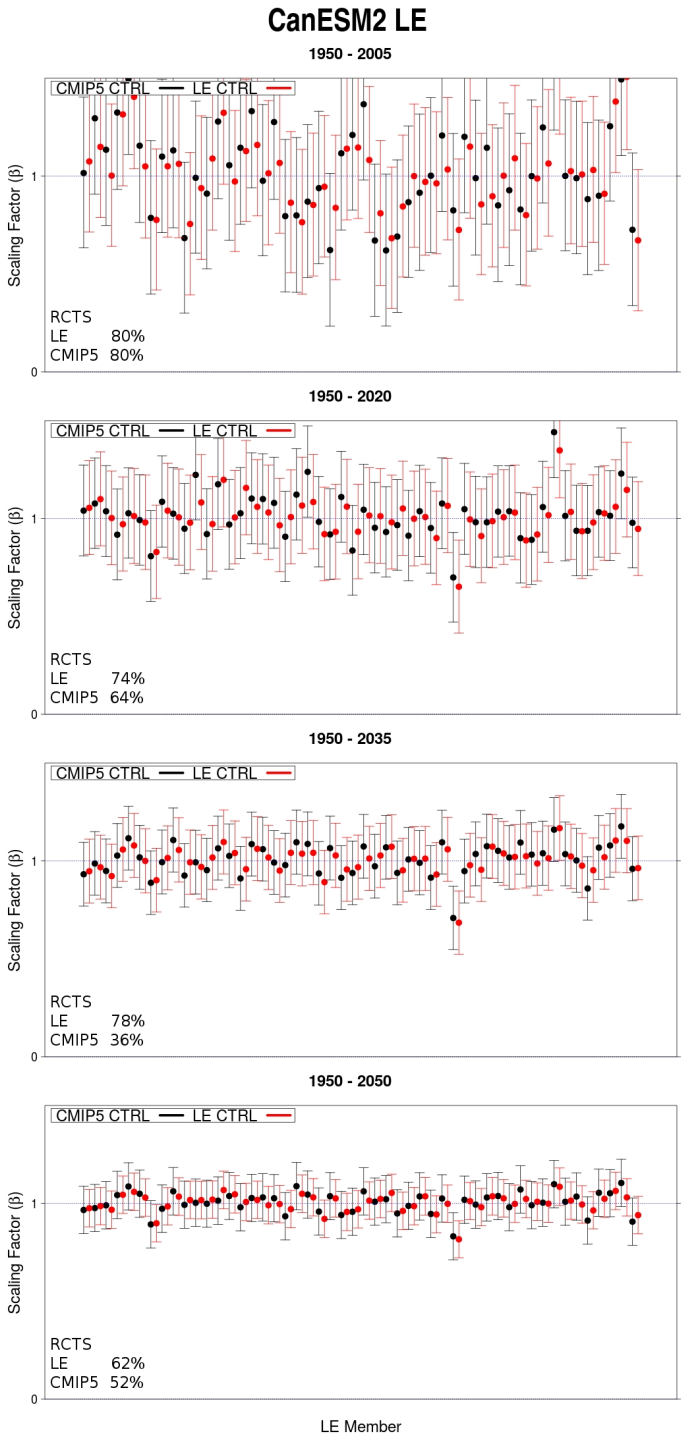

Figure 3.1: DA results from one-signal (ALL) perfect model analysis of Arctic September SIE using CanESM2 LE output. One ensemble member was treated as "observation" regressed on the fingerprint from all-but-one remaining LE members. Internal variability is estimated from either CMIP5 control runs (black) or from time series of residual variability from CanESM2 LE historical simulations (red). Dots represent the estimated scaling factor β; whiskers illustrates the 90% confidence interval. The success score for passing the RCT is given as *RCTS* when CMIP5 control variability or LE residual variability is used.

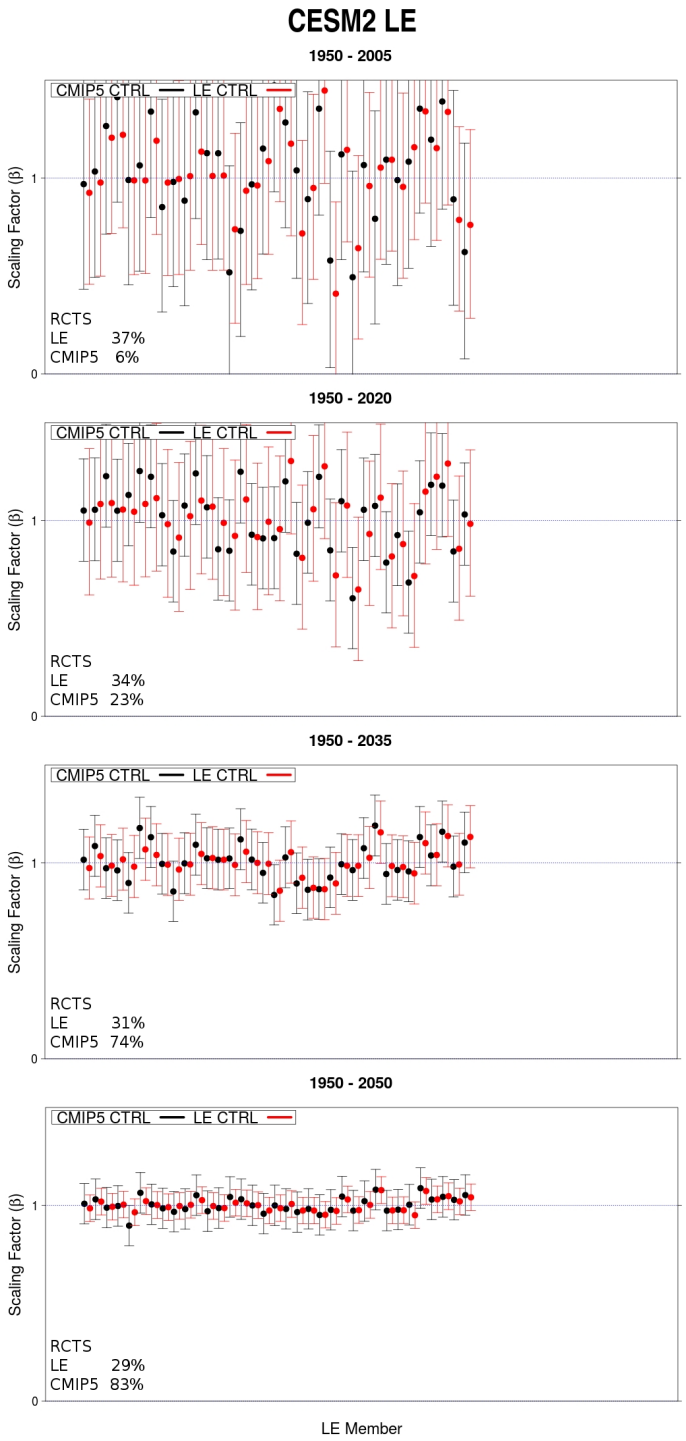

Figure 3.2: DA results from one-signal (ALL) perfect model analysis of Arctic September SIE using CESM LE output. One ensemble member was treated as "observation" regressed on the fingerprint from all-but-one remaining LE members. Internal variability is estimated from either CMIP5 control runs (black) or from time series of residual variability from CESM LE historical simulations (red). Dots represent the estimated scaling factor β; whiskers illustrates the 90% confidence interval. The analysis is repeated for four different time periods. The success score for passing the RCT is given as *RCTS* when CMIP5 control variability or LE residual variability is used.

For both LE the RCTS is about ten percent higher when IV2 is used instead of IV1.

In the second longest period from 1950 to 2035 the ALL signal from individual LE members is always detected in the ensemble mean for both PMEs. The uncertainty associated with corresponding beta terms is decreased compared to the two previous analysis periods. Only minimal differences in the scaling factors exist across the two models. The RCTS for both models are contradistinguished. For CanESM2 LE the RCT is passed in three-quarters of cases when using IV2. In CESM LE it is passed equally often when IV1 is used instead.

For the full available analysis period from 1950 to 2100 the ALL response is detected in all cases and with the smallest uncertainty range. The overall uncertainty ranges for estimated scaling factors in both models are smaller when IV2 is used instead of IV1.

Overall CanESM2 PME results seem to be independent from the choice of IV where CESM LE PME scaling factors are generally in closer agreement with unity when IV2 is used instead of IV1.

The PME results overall vary only little dependent on the choice of IV in all periods analysed. However, bigger differences exist in the achieved RCTS. Across models in six out of eight cases the RCTS is higher when transient IV2 is used. In the remaining two cases IV1 leads to higher passage rates. If the regression residuals of the DA study were to be random the RCT would be passed more often when the a independent sample estimate of the covariance matrix was constructed from unforced control runs (IV1). If the regression residual are distributed non-normally the test should fail more often on average. If internal variability changes conditional on the mean SIE then the regression residuals should be in closer agreement with an independent sample estimate of the covariance matrix constructed from transient ALL forcing runs (IV2).

The PME results give no strong indication that in the presented, contemporary, DA analysis period from 1953 to 2012 non-stationary internal variability has any influence on the robustness of estimated scaling factors. Differences in the RCTS exist but are rather small in the contemporary period. However, the PME results also suggest that the nonstationarity in Arctic internal sea ice variability is emerging in the recent decade and that future DA studies will have to address this change.

3.2 Detection and Attribution results

The DA results for the multi-model mean (MMM) response are shown in Figure 3.3. All three fingerprints from OANT, GHG and NAT forcing are detected in all three observed records (HADISST2, WC, PP) at the 10% significance level. The detection results for the MMM are consistent when using the two different estimates of internal variability IV1 and IV2. Minimal differences between the WC and PP data sets are reflected in the similarity of the estimated scaling factors. The simulated sea ice response under GHG forcing is in closest agreement with the observed changes in September Arctic sea ice extent (i.e. scaling factors closest to unity) for all data sets while exhibiting the narrowest uncertainty ranges of the 90% CI. The response to NAT is detected in all observation of Arctic SIE. However, the associated uncertainty range is larger for the weak NAT forcing in all data sets. Using IV2 for internal variability minimally increases uncertainty into estimated scaling factors under all three forcings. The WC data set fails the RCT when using IV2 while it is passed using the HadISST2 or PP data set as observation.

The DA results for individual CMIP5 models when using IV1 are presented here in Figure 3.4 and in Figure 3.5 when using IV2. A brief summary for each model's performance is given in the next paragraphs in alphabetic order. It is worth noting that signals from some models are estimated from a single or very few simulations. When looking at the results for individual models it is striking that the majority of scaling factors with open confidence belong to signals estimated from three or less simulations.

BBC-CSM-1-1 fingerprints for OANT, GHG and NAT are detectable in WC and PP observations under IV1. The RCT fails when HadISST2 and WC is used as observation. Under IV2 signals for OANT, GHG and NAT are detected in all observations and only when using HadISST2 fails the RCT. Scaling factors are closer to unity when IV2 is used. The NAT signal is closest to not being detected (scaling factor closest to zero) when IV1 is used.

Fingerprints for OANT, GHG and NAT from CanESM2 are detected in all observations and when either using IV1 or IV2. The RCT is plassed in all cases. When using HadISST2 as observations scaling factors are closer to unity when IV1 is used. For WC and PP observations using IV2 results in scaling factors closer to unity.

For CNRM-CM5 fingerprints for OANT, GHG and NAT are also detected in all observations. The RCT is passed in all cases. The results for IV1 and IV2 are almost

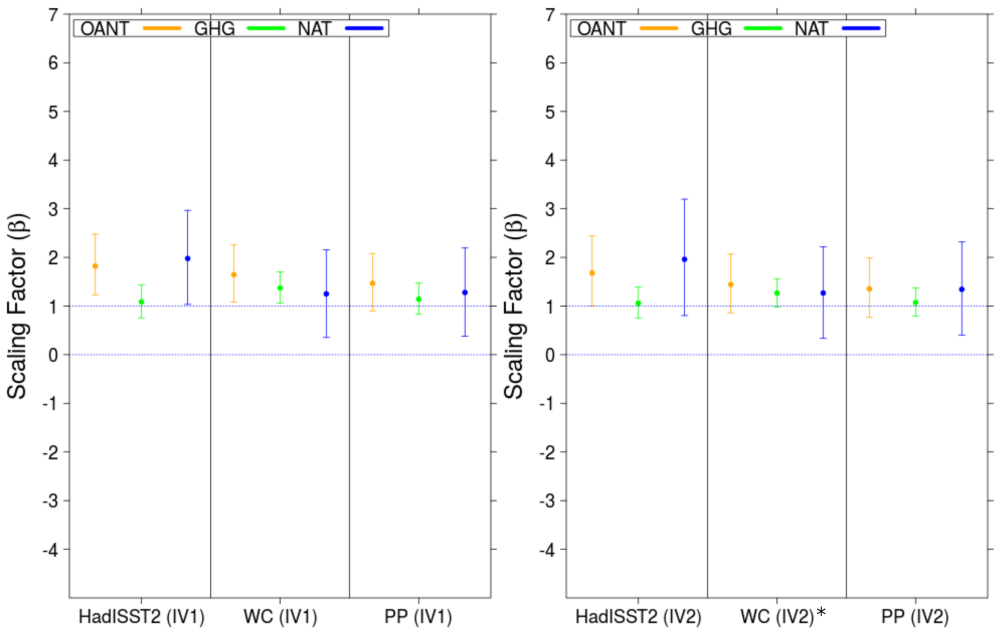

Figure 3.3: Detection and Attribution results for the multi-model mean show estimated scaling factors (dots) when three available observed data sets of September Arctic sea ice extent are regressed onto model derived fingerprints under GHG, ALL and NAT forcing and their 90% confidence intervals (whiskers). OANT is calculated following [46]. Calculation are shown in Table 3.1. The left panel shows results using IV1 to estimate internal variability. The right panel shows results using IV2 to estimate internal variability. An asterisk denotes failure of the residual consistency test at the 10% significance level.

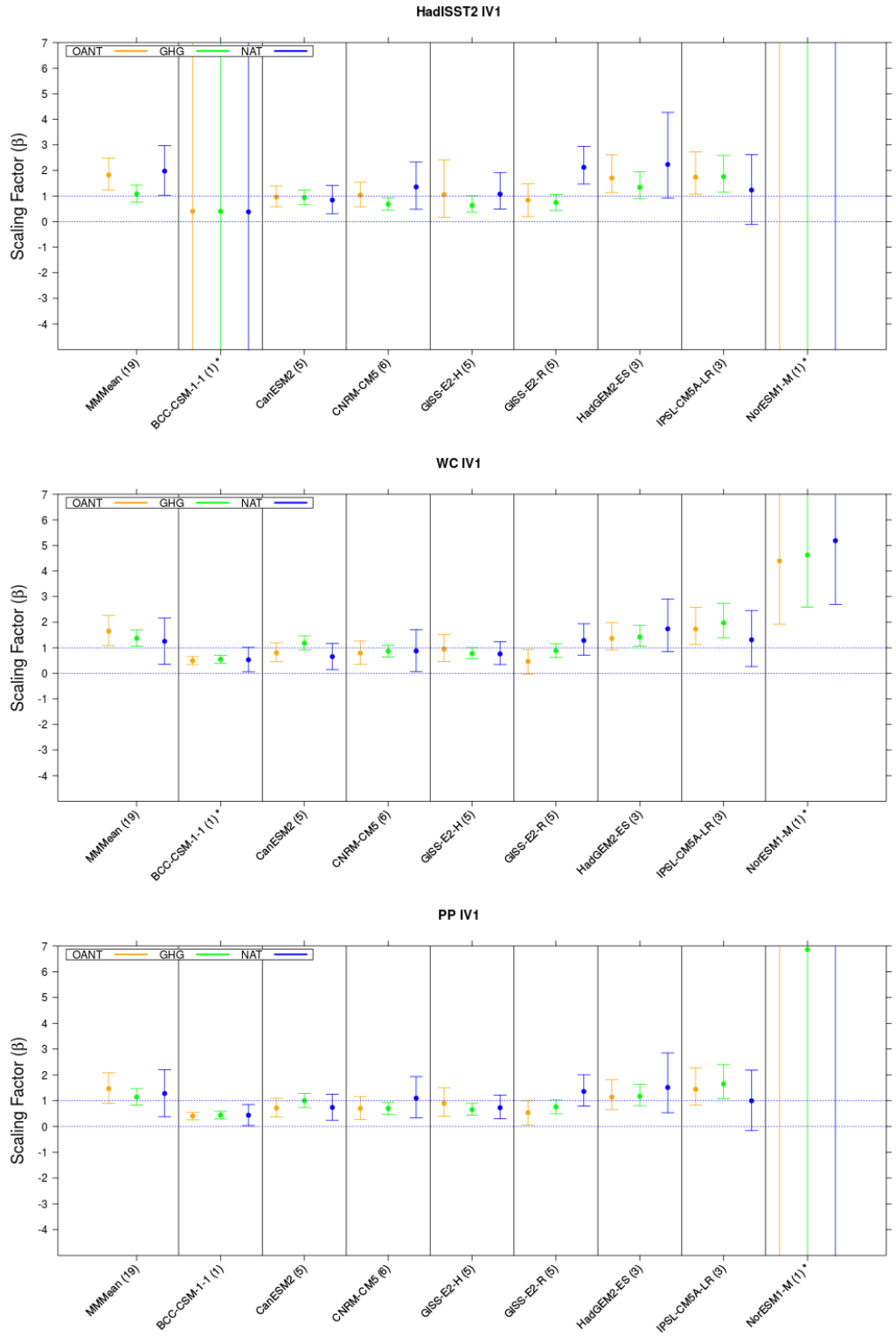

Figure 3.4: Detection results for individual models show estimated scaling factors by which model-derived fingerprints of September Arctic sea ice extent under OANT, GHG and NAT forcing need to be multiplied to best match the observations (HADISST2, WC, PP) and their 90% confidence interval using IV1 (constant) to estimate internal variability. An asterisk denotes failure of the residual consistency test at the 10% significance level.

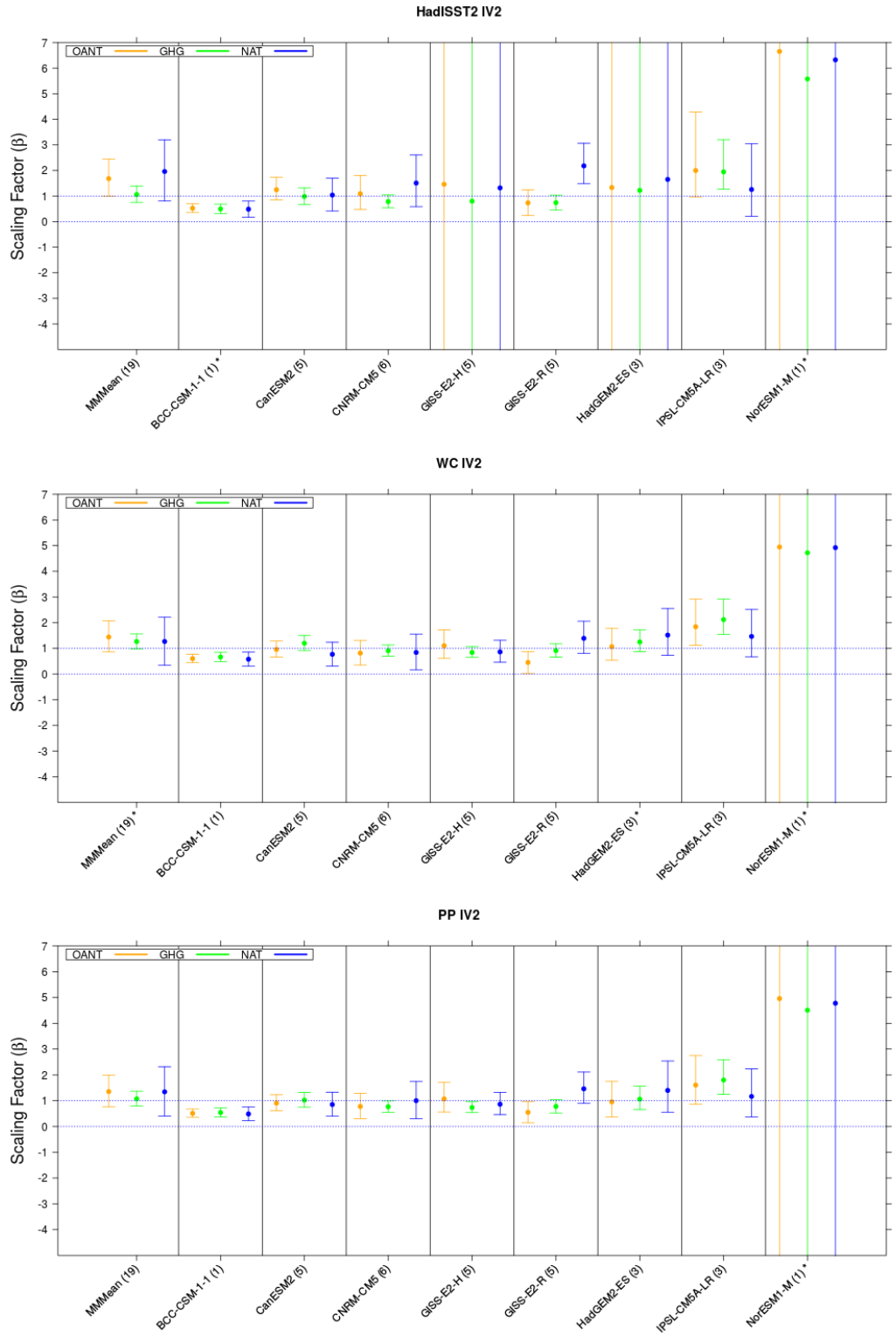

Figure 3.5: Detection results for individual models show estimated scaling factors by which model-derived fingerprints of September Arctic sea ice extent under OANT, GHG and NAT forcing need to be multiplied to best match the observations (HADISST2, WC, PP) and their 90% confidence interval using IV2 (non-stationary) to estimate internal variability. An asterisk denotes failure of the residual consistency test at the 10% significance level.

indistinguishable from each other.

When using GISS-E2-H simulations fingerprints for OANT, GHG and NAT are detected in all observation when using IV1. Fingerprints are detected in WC and PP observations when IV2 is used. The RCT fails for HadISST2 under IV2 and is passed in all other cases. Scaling factors for all three signals have open CIs when HadISST2. Uncertainty range is also largest for that observational data set under IV1, yet bounded.

In GISS-E2-R the fingerprint from ONAT is not detected in WC when IV1 is used. When IV2 is used all signals are detected in all observations. The RCT is passed in all cases.

Fingerprints for OANT, GHG and NAT derived from HadGEM2-ES are detected in all observations when IV1 is used. The RCT is passed for all observations, too. When using transient IV2 OANT, GHG and NAT signals are only detected in WC and PP. Scaling factors for HadISST2 have unbound CIs. However, scaling factors are in closer agreement with unity when IV2 is used.

The NorESM1-M model provided only one simulation under NAT and GHG forcing. Scaling factors for all forcings are outside the range of all other models in every case. In most cases CIs are unbounded and the RCT fails in every case. However, scaling factors are closer to unity when IV2 is used instead of IV1. The results are hard to interpret with just one simulation under each forcing.

In a next step we compare the observed trend of Arctic sea ice decline between 1953 – 2012 with the trend from the multi-model mean response under GHG, ALL and NAT forcing from which we calculate the contribution from OANT forcing (see Table 3.1). Here we only consider the observational record WC since it includes more information than HadISST2 and shows only marginal differences to the PP data compilation.

Finally, sea ice trends over 1953 – 2012 that are attributable to GHG, OANT and NAT are calculated by multiplying the trends in the multi-model mean forced responses by the estimated scaling factors from the DA results. The attributable trends for the CMIP5 multi-model mean response and WC trends are shown in Figure 3.6. More detailed results are shown in Table 3.2.

Figure 3.6 shows that the best estimate of the trend attributable to NAT forcing is roughly zero which is consistent with the expectation of quasi-random long term forcing variability. The trend attributable to GHG forcing is more negative than the observed negative trend of Arctic sea ice decline in the WC data. The difference can

Table 3.1: Modelled and observed trends of Arctic sea ice decline 1953 - 2012 in September.

CMIP5 forcing	-2σ	Trend $[\frac{10^6 km^2}{yr}]$	$+2\sigma$
GHG	-0.101	-0.064	-0.026
ALL	-0.091	-0.049	-0.008
NAT	-0.021	0.000	0.021
$OANT$[1]	0.031	0.015	-0.003
Observation		Trend $[\frac{10^6 km^2}{yr}]$	
WC		-0.053	

[1] $OANT = ALL - GHG - NAT$

Table 3.2: Scaling factors β and 5-95% confidence intervals ($\beta_{low} - \beta_{up}$) and corresponding attributable trends (AT)

CMIP5 forcing	β_{low}	β	β_{up}
GHG	1.059	1.371	1.704
$OANT$	1.082	1.645	2.260
NAT	0.353	1.251	2.156
Forcing	AT_{low}	AT $[\frac{10^6 km^2}{yr}]$	AT_{up}
GHG	-0.068	-0.088	-0.109
$OANT$	0.016	0.025	0.032
NAT	0.000	0.000	-0.000
ALL[2]	-0.052	-0.063	-0.077
$GHG + NAT$	-0.068	-0.088	-0.109

[2] $ALL = GHG + NAT + OANT$

be explained by a small positive annual sea ice trend attributable to the response to OANT forcing.

Thus we estimate that the effect from GHG and NAT forcing alone would have resulted in a much higher negative sea ice extent trend in Arctic sea ice simulations of $-0.088[10^6 km^2 * yr^{-1}]$ ($-0.107[10^6 km^2 * yr^{-1}]$ to $-0.044[10^6 km^2 * yr^{-1}]$) compared to $-0.063[10^6 km^2 * yr^{-1}]$ ($-0.080[10^6 km^2 * yr^{-1}]$ to $-0.006[10^6 km^2 * yr^{-1}]$) under ALL forcing. This means that roughly 30% of the decline has been offset by the combined cooling effect from OANT forcing.

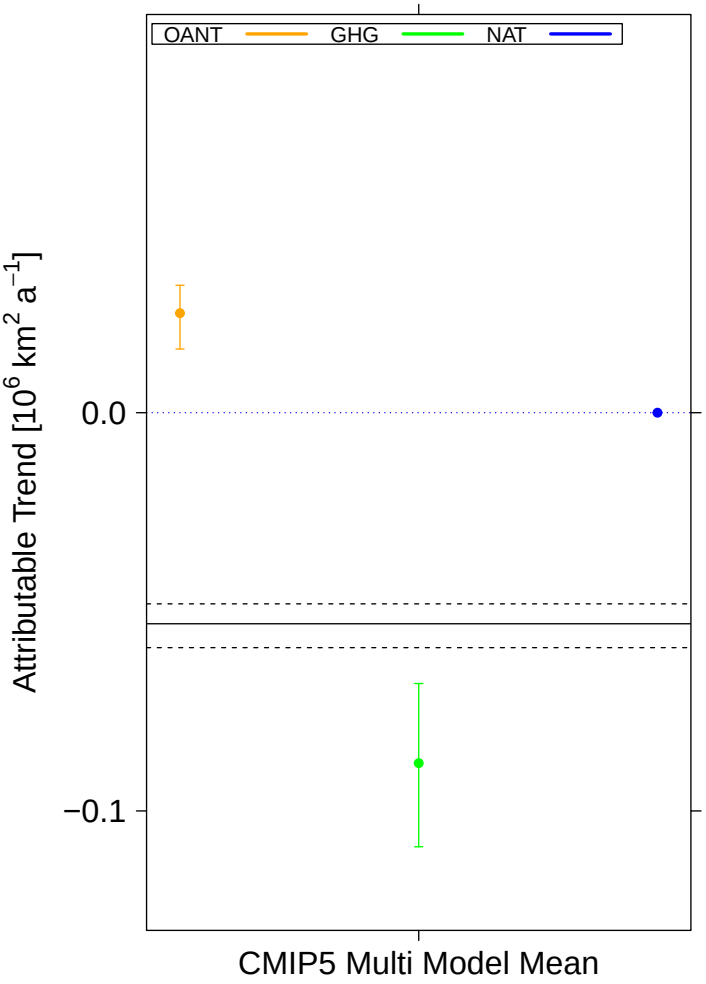

Figure 3.6: Arctic sea ice trends (in $10^6 km^2$ per year) attributable to OANT, GHG and NAT forcing. The solid horizontal line indicates the observed sea ice trend from the WC dataset and its 90% CI (dashed line).

Chapter 4

Discussion

The overall quality of the presented DA study is predominantly limited to times where reliable (i.e. spatially and temporally consistent) observations of Arctic sea ice exist. Any 'observational' data that is subject to climatological infill (e.g. early HadISST sea ice data) is generally not suitable for DA. Hence, all datasets used in this study are limited to the 1953 to 2012 period where full temporal and spatial coverage exists.

Quality is also limited by the climate models that I use. Climate models represent many of the physical processes that control sea ice formation e.g., melt, transport and deformation, but many subgrid-scale processes must be parameterized and the development of more complex and higher resolution climate models is far from complete. The selection of the sub-group of CMIP5 models used in this study was predominantly driven by the criterion of providing at least one simulation under ALL, GHG and NAT forcing experiments. The *CSIRO-MK-360* model was excluded because of concerns about the reliability of its sea ice simulation. For future generations of CMIP where more models provide larger ensembles under desired forcing experiments, aspects of model selection and model codependencies could deserve some reflection.

I find that when looking at the multi-model mean response of the CMIP5 models under investigation, fingerprints from GHG, OANT and NAT forcing can be detected in all three observational data sets of Arctic SIE in September. For the first time we detect the response to both OANT and NAT forcing in the observed Arctic SIE records using a formal DA approach. Modelled fingerprints are in closest agreement with the observed Arctic SIE in the PP data record (scaling factors closest to unity). The strong similarity between PP and WC sea ice fields is also reflected in the DA results. When the HadISST2 data set is used all fingerprints are also detected. However, in HadISST2 sea ice information from the Russian sector of the Arctic relies on an

outdated release of WC and does not yet include the more refined AARI sea ice information. This additional observational uncertainty may be a reason for stronger deviations between modelled and observed sea ice fields in the case of HadISST2.

As noted before the variability of SIE is not stationary. Therefore the covariance matrix of internal variability, a key element of the DA framework, was estimated in two ways (IV1, IV2) to test the sensitivity of the DA results to transience in the characteristics of the underlying IV. When comparing the DA result between the two sets of estimated internal climate variability (IV1, IV2) for the CMIP5 MME, no striking differences can be identified for the analysis period. Also, when looking at individual models the DA results the signal detection is generally not sensitive to the choice of IV and results vary only sightly (i.e. *IPSL-CM5A-LR*, see Figure 3.4 and 3.5).

The perfect model DA results for the 1950 to 2020 analysis period have the biggest overlap with the real world DA analysis period covering 1953 to 2012. No noticeable differences in the ALL signal detection frequency and accuracy are apparent that could be attributed to the choice of the IV estimate. However, the RCT scores indicate an overall higher failure rate than would be conceptionally expected from using a 90% confidence interval for the RCT. This renders the RCT test statistics used in ROF somewhat conservative. Despite the fact that the increasingly non-stationary IV acting upon Arctic sea ice is unfolding in the contemporary decade (Figure 3.1 3.2), its effect on our DA study covering 1953 – 2012, while present, is small. However, DA methods based on linear regression might be limited, especially in the context of SIE, due to increasingly non-stationary internal variability in the near term future and alternative approaches will become more applicable [55].

The results of the presented study demonstrate that available model simulation conducted for CMIP5 can be used to carry out a formal DA study on observed September SIE decline over the 1953 to 2012 period. By using new observational datasets that extend back into the pre-satellite era we are able to detect the climate response to natural-only (NAT) and other anthropogenic (OANT), mainly aerosols, forcing alongside the expected decline due to increased greenhouse-gas (GHG) forcing.

The combined cooling effect from OANT forcing is detectable in all three available datasets consistent with previous studies on aerosol offsetting of Arctic temperatures [46]. If technological advance and pollution control politics will reverse global aerosols burden it may be that whatever GHG-induced atmospheric warming has been masked by the rising levels of aerosols will then be exposed [31, 37].

A similar connection may exist considering future Arctic sea ice condition. With large uncertainty, OANT has offset about 30% of the decline that would have been expected in the absence of OANT forcing due to the combined climate response from GHG and NAT forcing. Future reduction of aerosol emissions may result in additional sea ice decline due to the reduced cooling effect.

The detection of a natural external (NAT) forcing in the observed records of September Arctic sea ice extent could be potentially linked to temporary cooling from volcanic forcing and the associated increase of stratospheric aerosols[12].

Beyond the relevance for the estimation of the covariance matrix of internal climate variability in the DA formalism some DA related studies make use of unforced control simulations for constraining future projections of the climate system [2, 68] and the likelihood of extreme events [71]. In both cases the internal variability is assumed to be stationary by using unforced control simulations that are then used to project future climate conditions. This practice would suffer if the internal variability is in fact non-stationary. Both approaches could be revisited using large ensemble perfect model approaches to test their working assumptions.

In this study we analyse model output from eight CMIP5 models that provided at least one simulation under GHG, ALL and NAT climate forcing for the 1953 to 2012 period and exclude one model from the analysis for its unrealistic sea ice simulations properties. The next phase of coupled model comparison, CMIP6, should provide a better experimental design and more realizations under different forcing [16], including special aerosol-only simulations that can be utilized to follow-up on the question of how Arctic sea ice condition will evolve in the future under changing aerosol emissions.

Bibliography

[1] MR Allen and PA Stott. Estimating signal amplitudes in optimal fingerprinting, part i: Theory. *Climate Dynamics*, 21(5-6):477–491, 2003.

[2] Myles R Allen, Peter A Stott, John FB Mitchell, Reiner Schnur, and Thomas L Delworth. Quantifying the uncertainty in forecasts of anthropogenic climate change. *Nature*, 407(6804):617–620, 2000.

[3] Haas C Bajish CC, Pittana M. Evaluation of arctic sea ice variability in cansise large ensemble of canesm-2. unpublished, 2015.

[4] Nathaniel L Bindoff, Peter A Stott, M AchutaRao, Myles R Allen, N Gillett, David Gutzler, Kabumbwe Hansingo, G Hegerl, Yongyun Hu, Suman Jain, et al. Detection and attribution of climate change: from global to regional. 2013.

[5] W. L. Chapman and J. E. Walsh. 20th-century sea-ice variations from observational data. *Annals of Glaciology*, 33(1):444–448, 1996.

[6] Josefino C Comiso, Donald J Cavalieri, Claire L Parkinson, and Per Gloersen. Passive microwave algorithms for sea ice concentration: A comparison of two techniques. *Remote sensing of Environment*, 60(3):357–384, 1997.

[7] Josefino C Comiso, Claire L Parkinson, Robert Gersten, and Larry Stock. Accelerated decline in the arctic sea ice cover. *Geophysical Research Letters*, 35(1), 2008.

[8] V Eyring, JM Arblaster, I Cionni, J Sedláček, Judith Perlwitz, PJ Young, Slimane Bekki, D Bergmann, Philip Cameron-Smith, William J Collins, et al. Long-term ozone changes and associated climate impacts in cmip5 simulations. *Journal of Geophysical Research: Atmospheres*, 118(10):5029–5060, 2013.

[9] F. Fetterer, K Knowles, W. Meier, and M. Savoie. Sea ice index, version 1. *NSIDC: National Snow and Ice Data Center*, 2002.

[10] Florence Fetterer, John Walsh, William Chapman, and J Scott Stewart. Sea ice back to 1850: A longer observational record for assimilation by models and use in reanalyses. In *EGU General Assembly Conference Abstracts*, volume 18, page 5157, 2016.

[11] JC Fyfe, K von Salzen, JNS Cole, NP Gillett, and J-P Vernier. Surface response to stratospheric aerosol changes in a coupled atmosphere–ocean model. *Geophysical Research Letters*, 40(3):584–588, 2013.

[12] John C Fyfe, Nathan P Gillett, and Francis W Zwiers. Overestimated global warming over the past 20 years. *Nature Climate Change*, 3(9):767–769, 2013.

[13] M-È Gagné, NP Gillett, and JC Fyfe. Impact of aerosol emission controls on future arctic sea ice cover. *Geophysical Research Letters*, 42(20):8481–8488, 2015.

[14] Nathan P Gillett, Vivek K Arora, Damon Matthews, and Myles R Allen. Constraining the ratio of global warming to cumulative co2 emissions using cmip5 simulations*. *Journal of Climate*, 26(18):6844–6858, 2013.

[15] Nathan P Gillett, Gabriele C Hegerl, Myles R Allen, and Peter A Stott. Implications of changes in the northern hemisphere circulation for the detection of anthropogenic climate change. *Geophysical research letters*, 27(7):993–996, 2000.

[16] Nathan P Gillett, Hideo Shiogama, Bernd Funke, Gabriele Hegerl, Reto Knutti, Katja Matthes, Benjamin D Santer, Daithi Stone, and Claudia Tebaldi. Detection and attribution model intercomparison project (damip). *Geoscientific Model Development Discussions*, pages 1–19, 2016.

[17] Nathan P Gillett, Francis W Zwiers, Andrew J Weaver, and Peter A Stott. Detection of human influence on sea-level pressure. *Nature*, 422(6929):292–294, 2003.

[18] NP Gillett, MF Wehner, SFB Tett, and AJ Weaver. Testing the linearity of the response to combined greenhouse gas and sulfate aerosol forcing. *Geophysical Research Letters*, 31(14), 2004.

[19] Hal B Gordon, Siobhan O'Farrell, Mark Collier, Martin Dix, Leon Rotstayn, Eva Kowalczyk, Tony Hirst, and Ian Watterson. *The CSIRO Mk3. 5 climate model*. CSIRO and Bureau of Meteorology, 2010.

[20] JM Gregory, PA Stott, DJ Cresswell, NA Rayner, C Gordon, and DMH Sexton. Recent and future changes in arctic sea ice simulated by the hadcm3 aogcm. *Geophysical Research Letters*, 29(24), 2002.

[21] David J Griggs and Maria Noguer. Climate change 2001: the scientific basis. contribution of working group i to the third assessment report of the intergovernmental panel on climate change. *Weather*, 57(8):267–269, 2002.

[22] Klaus Hasselmann. Optimal fingerprints for the detection of time-dependent climate change. *Journal of Climate*, 6(10):1957–1971, 1993.

[23] Klaus Hasselmann. Multi-pattern fingerprint method for detection and attribution of climate change. *Climate Dynamics*, 13(9):601–611, 1997.

[24] Gabriele C Hegerl, Klaus Hasselmann, U Cubasch, JFB Mitchell, E Roeckner, R Voss, and J Waszkewitz. Multi-fingerprint detection and attribution analysis of greenhouse gas, greenhouse gas-plus-aerosol and solar forced climate change. *Climate Dynamics*, 13(9):613–634, 1997.

[25] Gabriele C Hegerl, Ove Hoegh-Guldberg, Gino Casassa, Martin P Hoerling, RS Kovats, Camille Parmesan, David W Pierce, and Peter A Stott. Good practice guidance paper on detection and attribution related to anthropogenic climate change. In *Meeting Report of the Intergovernmental Panel on Climate Change Expert Meeting on Detection and Attribution of Anthropogenic Climate Change*, page 8. Citeseer, 2010.

[26] Gabriele C Hegerl, HANs voN SToRcH, Klaus Hasselmann, Benjamin D Santer, Ulrich Cubasch, and Philip D Jones. Detecting greenhouse-gas-induced climate change with an optimal fingerprint method. *Journal of Climate*, 9(10):2281–2306, 1996.

[27] Joonghyeok Heo and Seung-Ki Min. Attribution of recent arctic sea ice melting to human influence. In *EGU General Assembly Conference Abstracts*, volume 16, page 4647, 2014.

[28] William Richard Hobbs, Nathaniel L Bindoff, and Marilyn N Raphael. New perspectives on observed and simulated antarctic sea ice extent trends using optimal fingerprinting techniques*. *Journal of Climate*, 28(4):1543–1560, 2015.

[29] Gareth S Jones, Peter A Stott, and Nikolaos Christidis. Attribution of observed historical near–surface temperature variations to anthropogenic and natural causes using cmip5 simulations. *Journal of Geophysical Research: Atmospheres*, 118(10):4001–4024, 2013.

[30] JE Kay, C Deser, A Phillips, A Mai, C Hannay, G Strand, JM Arblaster, SC Bates, G Danabasoglu, J Edwards, et al. The community earth system model (cesm) large ensemble project: A community resource for studying climate change in the presence of internal climate variability. *Bulletin of the American Meteorological Society*, 96(8):1333–1349, 2015.

[31] Silvia Kloster, Frank Dentener, Johann Feichter, Frank Raes, Ulrike Lohmann, Erich Roeckner, and Irene Fischer-Bruns. A gcm study of future climate response to aerosol pollution reductions. *Climate dynamics*, 34(7-8):1177–1194, 2010.

[32] Thomas R Knutson, Fanrong Zeng, and Andrew T Wittenberg. Multimodel assessment of regional surface temperature trends: Cmip3 and cmip5 twentieth-century simulations. *Journal of Climate*, 26(22):8709–8743, 2013.

[33] R Kwok and DA Rothrock. Decline in arctic sea ice thickness from submarine and icesat records: 1958–2008. *Geophysical Research Letters*, 36(15), 2009.

[34] R Kwok, G Spreen, and S Pang. Arctic sea ice circulation and drift speed: Decadal trends and ocean currents. *Journal of Geophysical Research: Oceans*, 118(5):2408–2425, 2013.

[35] Seymour W Laxon, Katharine A Giles, Andy L Ridout, Duncan J Wingham, Rosemary Willatt, Robert Cullen, Ron Kwok, Axel Schweiger, Jinlun Zhang, Christian Haas, et al. Cryosat-2 estimates of arctic sea ice thickness and volume. *Geophysical Research Letters*, 40(4):732–737, 2013.

[36] Olivier Ledoit and Michael Wolf. A well-conditioned estimator for large-dimensional covariance matrices. *Journal of multivariate analysis*, 88(2):365–411, 2004.

[37] Hiram Levy, Larry W Horowitz, M Daniel Schwarzkopf, Yi Ming, Jean-Christophe Golaz, Vaishali Naik, and V Ramaswamy. The roles of aerosol direct and indirect effects in past and future climate change. *Journal of Geophysical Research: Atmospheres*, 118(10):4521–4532, 2013.

[38] RW Lindsay, J Zhang, A Schweiger, M Steele, and H Stern. Arctic sea ice retreat in 2007 follows thinning trend. *Journal of Climate*, 22(1):165–176, 2009.

[39] Andrew R Mahoney, Roger G Barry, Vasily Smolyanitsky, and Florence Fetterer. Observed sea ice extent in the russian arctic, 1933–2006. *Journal of Geophysical Research: Oceans*, 113(C11), 2008.

[40] François Massonnet, Thierry Fichefet, Hugues Goosse, Cecilia M Bitz, Gwenaëlle Philippon-Berthier, Marika M Holland, and P-Y Barriat. Constraining projections of summer arctic sea ice. *The Cryosphere*, 6(6):1383–1394, 2012.

[41] Walter N Meier, Julienne Stroeve, Andrew Barrett, and Florence Fetterer. A simple approach to providing a more consistent arctic sea ice extent timeseries from the 1950s to present. *The Cryosphere Discussions*, 6(4):2827–2853, 2012.

[42] William J Merryfield, Woo-Sung Lee, George J Boer, Viatcheslav V Kharin, John F Scinocca, Gregory M Flato, RS Ajayamohan, John C Fyfe, Youmin Tang, and Saroja Polavarapu. The canadian seasonal to interannual prediction system. part i: Models and initialization. *Monthly weather review*, 141(8):2910–2945, 2013.

[43] Seung-Ki Min, Xuebin Zhang, Francis W Zwiers, and Tom Agnew. Human influence on arctic sea ice detectable from early 1990s onwards. *Geophysical Research Letters*, 35(21), 2008.

[44] Seung-Ki Min, Xuebin Zhang, Francis W Zwiers, and Gabriele C Hegerl. Human contribution to more-intense precipitation extremes. *Nature*, 470(7334):378–381, 2011.

[45] John Mitchell, D Karoly, Gabi Hegrel, Francis Zwiers, Myles Allen, and Jose Marengo. Detection of climate change and attribution of causes. 2001.

[46] Mohammad Reza Najafi, Francis W Zwiers, and Nathan P Gillett. Attribution of arctic temperature change to greenhouse-gas and aerosol influences. *Nature Climate Change*, 2015.

[47] Mohammad Reza Najafi, Francis W Zwiers, and Nathan P Gillett. Attribution of the spring snow cover extent decline in the northern hemisphere, eurasia and north america to anthropogenic influence. *Climatic Change*, 136(3-4):571–586, 2016.

[48] Miguel Ángel Cea Pirón and Juan Antonio Cano Pasalodos. Nueva serie de extensión del hielo marino ártico en septiembre entre 1935 y 2014. *REVISTA DE CLIMATOLOGÍA*, 16, 2016.

[49] Serge Planton, Armineh Barkhordarian, Aurélien Ribes, and Hans Von Storch. Detection and attribution. In *Regional Assessment of Climate Change in the Mediterranean*, pages 157–186. Springer, 2013.

[50] Igor V Polyakov, Genrikh V Alekseev, Roman V Bekryaev, Uma S Bhatt, Roger Colony, Mark A Johnson, Valerii P Karklin, David Walsh, and Alexander V Yulin. Long-term ice variability in arctic marginal seas. *Journal of Climate*, 16(12):2078–2085, 2003.

[51] Aurélien Ribes, Jean-Marc Azaïs, and Serge Planton. Adaptation of the optimal fingerprint method for climate change detection using a well-conditioned covariance matrix estimate. *Climate Dynamics*, 33(5):707–722, 2009.

[52] Aurélien Ribes, Nathan P Gillett, and Francis W Zwiers. Designing detection and attribution simulations for cmip6 to optimize the estimation of greenhouse gas–induced warming. *Journal of Climate*, 28(8):3435–3438, 2015.

[53] Aurélien Ribes, Serge Planton, and Laurent Terray. Application of regularised optimal fingerprinting to attribution. part i: method, properties and idealised analysis. *Climate dynamics*, 41(11-12):2817–2836, 2013.

[54] Aurélien Ribes and Laurent Terray. Application of regularised optimal fingerprinting to attribution. part ii: application to global near-surface temperature. *Climate dynamics*, 41(11-12):2837–2853, 2013.

[55] Aurélien Ribes, Francis W Zwiers, Jean-Marc Azaïs, and Philippe Naveau. A new statistical approach to climate change detection and attribution. *Climate Dynamics*, pages 1–20, 2016.

[56] Alan Robock. Volcanic eruptions and climate. *Reviews of Geophysics*, 38(2):191–219, 2000.

[57] James M Rosinski and David L Williamson. The accumulation of rounding errors and port validation for global atmospheric models. *SIAM Journal on Scientific Computing*, 18(2):552–564, 1997.

[58] Drew A Rothrock, Yanling Yu, and Gary A Maykut. Thinning of the arctic sea-ice cover. *Geophysical Research Letters*, 26(23):3469–3472, 1999.

[59] David E Rupp, Philip W Mote, Nathaniel L Bindoff, Peter A Stott, and David A Robinson. Detection and attribution of observed changes in northern hemisphere spring snow cover. *Journal of Climate*, 26(18):6904–6914, 2013.

[60] Benjamin M Sanderson, Reto Knutti, and Peter Caldwell. A representative democracy to reduce interdependency in a multimodel ensemble. *Journal of Climate*, 28(13):5171–5194, 2015.

[61] Makiko Sato, James E Hansen, M Patrick McCormick, and James B Pollack. Stratospheric aerosol optical depths, 1850–1990. *Journal of Geophysical Research: Atmospheres*, 98(D12):22987–22994, 1993.

[62] V Selyuzhenok, Thomas Krumpen, A Mahoney, Markus Janout, and Rüdiger Gerdes. Seasonal and interannual variability of fast ice extent in the southeastern laptev sea between 1999 and 2013. *Journal of Geophysical Research: Oceans*, 2015.

[63] Mark C Serreze, Marika M Holland, and Julienne Stroeve. Perspectives on the arctic's shrinking sea-ice cover. *science*, 315(5818):1533–1536, 2007.

[64] Qi Shu, Zhenya Song, and Fangli Qiao. Assessment of sea ice simulations in the cmip5 models. *The Cryosphere*, 9(1):399–409, 2015.

[65] RB Skeie, TK Berntsen, G Myhre, K Tanaka, MM Kvalevåg, and CR Hoyle. Anthropogenic radiative forcing time series from pre-industrial times until 2010. *Atmospheric Chemistry and Physics*, 11(22):11827–11857, 2011.

[66] Susan Solomon, John S Daniel, R RIII Neely, J-P Vernier, Ellsworth G Dutton, and Larry W Thomason. The persistently variable background stratospheric aerosol layer and global climate change. *Science*, 333(6044):866–870, 2011.

[67] B Spagnoli, S Planton, M Déqué, O Mestre, and J-M Moisselin. Detecting climate change at a regional scale: the case of france. *Geophysical Research Letters*, 29(10), 2002.

[68] Peter A Stott and JA Kettleborough. Origins and estimates of uncertainty in predictions of twenty-first century temperature rise. *Nature*, 416(6882):723–726, 2002.

[69] Julienne C Stroeve, Vladimir Kattsov, Andrew Barrett, Mark Serreze, Tatiana Pavlova, Marika Holland, and Walter N Meier. Trends in arctic sea ice extent from cmip5, cmip3 and observations. *Geophysical Research Letters*, 39(16), 2012.

[70] Julienne C Stroeve, Mark C Serreze, Marika M Holland, Jennifer E Kay, James Malanik, and Andrew P Barrett. The arctics rapidly shrinking sea ice cover: a research synthesis. *Climatic Change*, 110(3-4):1005–1027, 2012.

[71] Ying Sun, Xuebin Zhang, Francis W Zwiers, Lianchun Song, Hui Wan, Ting Hu, Hong Yin, and Guoyu Ren. Rapid increase in the risk of extreme summer heat in eastern china. *Nature Climate Change*, 4(12):1082–1085, 2014.

[72] Neil C Swart, John C Fyfe, Ed Hawkins, Jennifer E Kay, and Alexandra Jahn. Influence of internal variability on arctic sea-ice trends. *Nature Climate Change*, 5(2):86–89, 2015.

[73] CT Swift and DJ Cavalieri. Passive microwave remote sensing for sea ice research. *Eos, Transactions American Geophysical Union*, 66(49):1210–1212, 1985.

[74] Karl E Taylor, V Balaji, Steve Hankin, Martin Juckes, Bryan Lawrence, and Stephen Pascoe. Cmip5 data reference syntax (drs) and controlled vocabularies, 2011.

[75] Simon FB Tett, Peter A Stott, Myles R Allen, William J Ingram, and John FB Mitchell. Causes of twentieth-century temperature change near the earth's surface. *Nature*, 399(6736):569–572, 1999.

[76] Holly A Titchner and Nick A Rayner. The met office hadley centre sea ice and sea surface temperature data set, version 2: 1. sea ice concentrations. *Journal of Geophysical Research: Atmospheres*, 119(6):2864–2889, 2014.

[77] P Uotila, S O'Farrell, SJ Marsland, and D Bi. The sea-ice performance of the australian climate models participating in the cmip5. *Australian Meteorological and Oceanographic Journal*, 63(1):121–143, 2013.

[78] David G Vaughan, Josefino C Comiso, Ian Allison, Jorge Carrasco, Georg Kaser, Ronald Kwok, Philip Mote, Tavi Murray, Frank Paul, Jiawen Ren, et al. Observations: cryosphere. *Climate change*, pages 317–382, 2013.

[79] Konstantin Y Vinnikov, Alan Robock, Ronald J Stouffer, John E Walsh, Claire L Parkinson, Donald J Cavalieri, John FB Mitchell, Donald Garrett, and Victor F Zakharov. Global warming and northern hemisphere sea ice extent. *Science*, 286(5446):1934–1937, 1999.

[80] John E Walsh and Claudia M Johnson. An analysis of arctic sea ice fluctuations, 1953-77. *Journal of Physical Oceanography*, 9(3):580–591, 1979.

[81] W. L. Chapman Walsh, J. E. and F. Fetterer. Gridded monthly sea ice extent and concentration, 1850 onward, version 1. *National Snow and Ice Data Center*, 2015.

[82] Hui Wan, Xuebin Zhang, Francis Zwiers, and Seung-Ki Min. Attributing northern high-latitude precipitation change over the period 1966–2005 to human influence. *Climate Dynamics*, 45(7-8):1713–1726, 2015.

[83] Francis W Zwiers, Gabriele C Hegerl, Xuebin Zhang, and Qiuzi Wen. Quantifying the human and natural contributions to observed climate change. *Statistics in Action: A Canadian Outlook*, page 321, 2014.